PV, Wind and Space Heating Electrification Utilization Analysis for a Small Canadian Arctic Hybrid Microgrid

Thomas Paulin-Bessette

A Thesis

In the Department of

Electrical and Computer Engineering

Presented in Partial Fulfillment of the Requirements

For the Degree of

Master of Applied Science (Electrical and Computer Engineering)

at Concordia University

Montreal, Quebec, Canada

July 2024

CONCORDIA UNIVERSITY

SCHOOL OF GRADUATE STUDIES

This is to certify that the thesis prepared

By: Thomas Paulin-Bessette

Entitled: PV, Wind and Space Heating Electrification Utilization Analysis for a Small Canadian Arctic Hybrid Microgrid

and submitted in partial fulfillment of the requirements for the degree of

Master of Applied Science (Electrical and Computer Engineering)

complies with the regulations of the University and meets the accepted standards with respect to originality and quality.

Signed by the final examining committee:

_____ Chair

Dr. Pragasen Pillay

_____ External Examiner

Dr. Mohamed Ouf

_____ Supervisor

Dr. Luiz A. C. Lopes

Approved by:

_____

Dr. Yousef R. Shayan, Department Chair

Department of Electrical and Computer Engineering

_____

Dr. Mourad Debbabi, Dean

Gina Cody School of Engineering and Computer Science

Date: August 14th 2024

Abstract

PV, Wind and Space Heating Electrification Utilization Analysis for a Small Canadian Arctic Hybrid Microgrid

Thomas Paulin-Bessette

Canadian Arctic remote communities mostly rely on diesel gensets (DGSs) to produce electricity, which is expensive and emits greenhouse gases (GHG) that pollute the environment and affect the air quality. These communities can utilize their renewable energy (RE) potential to reduce both their fuel consumption and the associated GHG emissions.

In the first part of the project, the potential of PV and wind turbines (WTs) is evaluated. The PV utilization analysis results in a contribution of nearly 22% of the yearly community energy requirement and diesel savings of up to 18% with a rated PV power of 200 kW or 125% of the community load peak power. As for the analysis of the wind system, the renewable energy contribution reaches close to 36% alongside fuel savings of 29% for three 25 kW WTs. When combining PV and WTs, the portion of energy supplied by the renewable energy (RE) system reaches 44% along with 36% fuel savings. However, when including RE to the microgrid, its penetration, or percentage of total energy provided by PV, and its associated fuel savings are limited by curtailment, to prevent the DGSs from operating with low loading.

The second part of the project evaluates the addition of electric thermal storage (ETS) to the microgrid, which allows for recycling excess (curtailed) RE production to electrify a portion of the heating requirements of the community which is currently oil-based. When pairing ETS units with WTs and PV, the RE curtailment is significantly reduced and can be lowered by up to 90% when ETS units are installed in all the houses of the considered community. Lastly, ETS units can increase the total fuel savings and associated GHG emissions by 46%, when compared to the first part of the study.

Acknowledgements

First, I would like to extend my deepest gratitude to Prof. Luiz A.C. Lopes without whom this project would not have been possible. Thank you for your time and your wise guidance. I have always been amazed by your patience, your attention to detail and your will to understand my project and my ideas fully and deeply so you could always give me the best advice. Thank you for your positivity and friendliness, it has been a great pleasure to work under your supervision. I hope we can keep collaborating in the future.

Next, I am profoundly grateful for my colleagues and managers at CanmetENERGY in Varennes who have provided me a perfect environment to expand my knowledge both academically and professionally. I would especially like to thank Nayeem, Marc, Indrajit, Yves and Véronique for your guidance and contribution to this project.

Then, I would like to thank Concordia University and the Professors and staff I have had the opportunity to meet during these last two years. You have taught me a lot and always advised me accurately. I would like to express my appreciation to Concordia University once again, along with The Natural Sciences and Engineering Research Council of Canada (NSERC) for their financial contributions throughout my master's studies.

Enfin, merci à ma conjointe Solène, à ma famille et à mes amis qui se sont intéressés à mon projet et qui m'ont supporté durant ma maîtrise.

Table of Contents

List of Figures

List of Tables

Abbreviations

AC: Alternative Current

DC: Direct Current

DGS: Diesel Genset

ETS: Electric Thermal Storage

E-W: East-West

GHG: Greenhouse gas

MPPT: Maximum Power Point Tracking

O&M: Operation & Maintenance

OS: Optimal South

PCC: Pearson Correlation Coefficient

PV: Photovoltaics

RE: Renewable Energy

TMY: Typical Meteorological Year

TT: Two-Tilt

WSM: Wind Speed Multiplier

WT: Wind Turbine

Chapter 1 - Introduction

1.1. Problem Statement and Proposed Solution

Canada has hundreds of remote communities, most of them Indigenous, that mainly rely on diesel to generate electricity, which is expensive, has an impact on the environment and affects air quality. The addition of RE in these communities can help reduce GHG emissions, provide healthier living conditions for the locals and savings to the communities [1], [2], [3]. This project follows the work done in [4], a generic study that aims to increase the penetration of PV (portion of energy supplied by PV) in a small Canadian Arctic PV-diesel hybrid microgrid to provide more RE energy thus reducing the pollution and GHG emissions while providing fuel savings that can be reinvested in the community. The first purpose of this study is to evaluate the effect of adding WTs, a new RE source, in the model presented in [4] and further reduce the GHG emissions associated to diesel compared to the original scenario.

Next, a second part of the study considers the electrification of space heating by installing ETS furnaces and charging them with excess RE production. Since RE production does not always match the load demand, some of it may be curtailed, or go to waste when there is no storage element, as in the first part of the study. This section will assess the potential of adding ETS units to both recycle the excess RE production that was wasted in the first study and use it to electrify a portion of the heating requirements of the buildings of the community, thus reducing the consumption of heating oil and the associated GHG emissions. The parameters considered in the study are: 1) RE penetration, 2) RE curtailment and 3) Diesel and Heating Oil fuel Consumption.

1.2. Thesis Contribution

The first part of the project will aim to answer challenges in the topic of combining WTs and PV in Arctic conditions that were identified through a literature review [5], [6], [7]. Among the identified issues, those considered in this study are detailed in the following sentences. First, RE integration studies for Arctic regions which consider existing systems suitable for arctic conditions are scarce. Indeed, microgrids located in Arctic regions are faced with unique challenges and require specific equipment that can sustain extreme cold and that is of reasonable size to be transported there, since some communities are only accessible by winter ice roads, by barge or by plane. Therefore, when assessing the potential of RE integration in Northern microgrids, it is essential to consider equipment and technology that is suitable for Arctic conditions. Additionally, there is a need to conduct location-specific studies because the best combination of PV and WTs is highly affected by the correlation between these energy sources and the load demand of the community. Furthermore, these communities all differ in terms of size, structure, geographical location, renewable resource availability and more [8]. Therefore, there is no unique solution to reduce their dependency on diesel and more cases configurations must be studied. The model developed in this study is modular and could be reused to evaluate the potential of RE integration for different communities with unique load profiles and RE resources. Lastly, there is a lack of

studies in the literature which include thermal loads as part as decarbonization scenarios and pathways for remote arctic microgrids. Indeed, in northern remote communities, thermal loads represent higher energy consumption than the electric grids powered by diesel generators [9], [10] and should therefore be considered when trying to reduce GHG emissions.

To evaluate the potential for RE integration in remote Arctic microgrids, different scenarios, with either WTs only or a combination of PV and WTs, are considered to reduce fuel consumption. However, RE added to microgrids can be curtailed due to its mismatch with the electricity demand as well as to the minimum loading requirement of Diesel Gensets (DGSs), limiting fuel savings. This curtailment, or capping of production, increases with more RE, especially for photovoltaic (PV) systems. Therefore, additional aspects, such as panel tilt and orientation, are also studied to determine if they can increase the penetration while limiting the curtailment of RE. All the power system elements modelled in this study are based on commercially available devices to ensure that the study is realistic and allows for the methodology to be applied in a real-life scenario.

Next, the thesis proposes a methodology to model the combination of space heating electrification and RE integration in an Arctic microgrid, where excess RE production is recycled to heat buildings. First, a detailed methodology was applied to model the yearly space heating requirements of a community using EnergyPlus based on satellite imagery, weather datasets and typical Arctic building models. Then, this thesis introduces Electric Thermal Storage (ETS), to supply a portion of the heating requirements of the community by recycling excess RE. Based on a thorough literature review of ETS modelling [10], [11], [12], [13], [14], [15], [16], [17], [18], [19], a lack of study in that field was identified. More specifically, studies evaluating the potential of ETS units in Arctic microgrid are scarce. Also, some of the identified models and studies do not consider the core temperature of ETS units, which has a direct effect on the heater's standby losses and available output power at a given moment. Both these elements are detailed and considered in the study. Lastly, studies considering the electrification of space heating in remote Arctic communities are essential to help with the overall decarbonization of these microgrids because heating represents a majority of their energy needs for buildings [9] and, in a great majority of cases, it is entirely generated with fossil fuels [20].

1.3. Thesis Outline

The technical content of the thesis is separated in three chapters. Chapter 2 describes the Diesel-RE hybrid microgrid model used for the study. It presents the input data used, the power system specifications, the microgrid control system and the model representation in MATLAB Simulink. Then, Chapter 3 presents the low penetration RE analysis, of a system with PV and/or WTs, without storage or load-side management. In this chapter, Diesel-PV, Diesel-WT and Diesel-PV-WTs configurations are considered. Some strategies aiming to reduce the curtailment of the PV system are also studied. Lastly, Chapter 4 proposes the electrification of a portion of the space heating of the community to recycle the excess RE production. The chapter contains the community space heating load modelling, the ETS modelling and how it is implemented in MATLAB Simulink as

well as an analysis of the results obtained when considering space heating electrification in a remote Diesel-PV-WT hybrid microgrid.

Chapter 2 - PV-Wind-Diesel Hybrid Microgrid Model

2.1. Input Model Data

2.1.1. Lumped Power Load

The yearly minute-level electrical load profile of the community is the same one used in [4]. The profile is presented in Figure 1; it has a minimum of 30 kW, an average of 73 kW and a maximum of 160 kW. The yearly community energy demand of the community is 639 MWh. Without RE, the yearly fuel consumption of the diesel power plant is 184 kL. The load profile considered in the study includes appliances and lighting. Thermal loads, such as space and water heating, are not part of the dataset since they are oil-based in this community. The increase of the electric demand during winter can be explained by the fact that more lighting and usage of the appliances is required when the days are shorter.

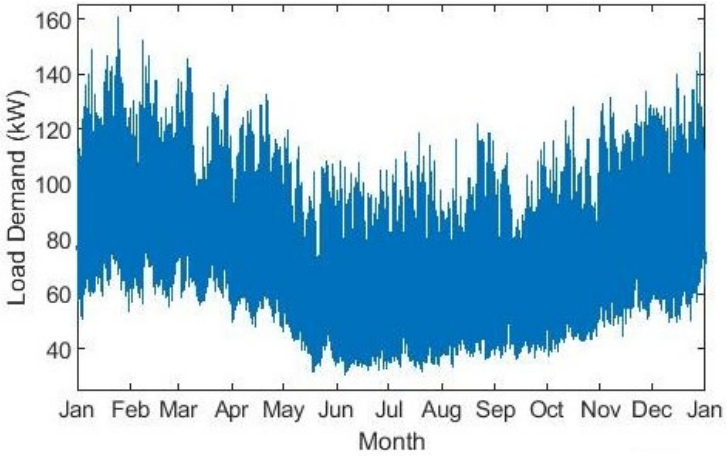

Figure 1 – Yearly Load Demand Profile

2.1.2. Weather Information

A yearly hour-level TMY solar irradiance profile from a small Canadian Arctic community (61° 6' 0" N, 94° 4' 12" W) is used for the PV system [21]. It is resampled to minute-level, using cubic interpolation, to match the load profile used in the simulation. A translation algorithm from PVLIB Python was used to obtain incident panel irradiance datasets. The first scenario considered is with south-facing panels with optimal tilt to maximize the yearly production. In the rest of the text, this scenario will be identified as Optimal South (OS). The angle of 48.8° was determined by testing numerous optimal tilt angle models presented in [22]. For the location considered in this study, the model which provides the most PV production is given by,

$$\beta = 7.203° + 0.6804(\phi) \quad (1)$$

where β is the panel tilt angle and ϕ is the latitude. The obtained incident irradiance profile is presented in Figure 2. The OS PV scenario has a maximum irradiance of 1141 W/m^2. It is the main input to the modelled PV system. A yearly hour-level temperature profile obtained from the same

TMY dataset is used in the model as an input to the PV system. A yearly hour-level wind speed profile from a Canadian Arctic community is obtained from Weather Canada [23], is used for the WT system. At the measured altitude of 18.6 m, the wind profile (Figure 3) has a yearly average speed of 5.84 m/s.

The simulation is done for a one-year period with a one-minute time step. As for the solar irradiance datasets, the wind speed data were resampled to minute-level, using cubic interpolation, to match the load profile.

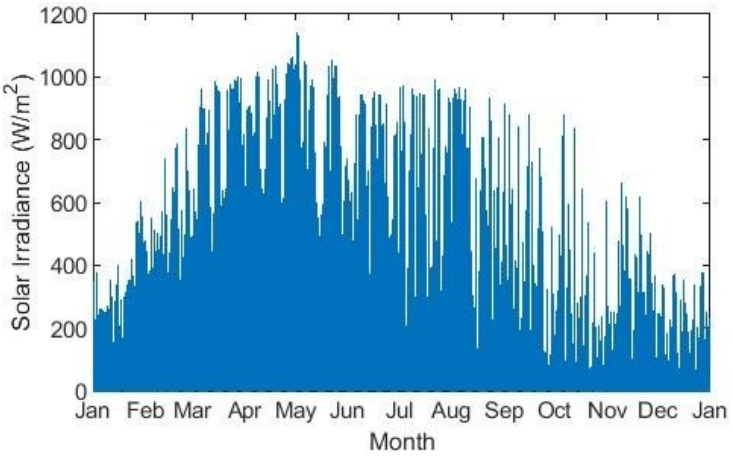

Figure 2 – Yearly Irradiance Profile – Optimal Tilt (48.8°)

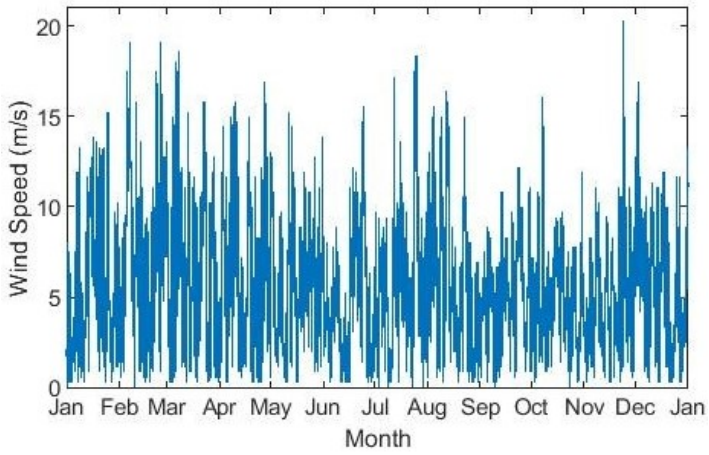

Figure 3 – Yearly Wind Speed Profile

2.2. Power System Specifications

CanmetENERGY-Varennes has developed a MATLAB/Simulink toolbox [24] for PV-based hybrid microgrid system simulation which has been used previously to model remote microgrid systems in [2], [25]. It is used to model elements of the power system considered in this study. The proposed system is presented below, in Figure 4.

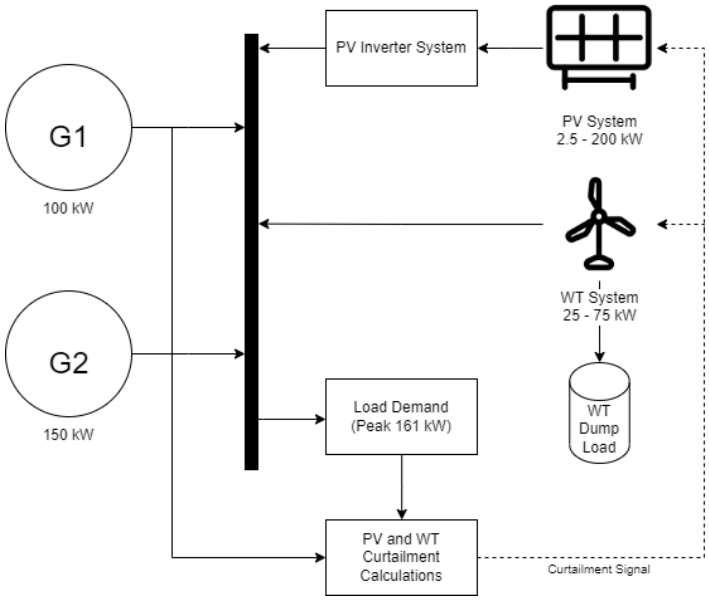

Figure 4 – Diagram of Modelled Power System

It consists of two diesel generators, one of 100 kW and the other of 150 kW, which supply the electric load demand of the community. To reduce the diesel consumption, the power plant is paired with both PV and WT systems. The PV system includes PV panels as well as inverters with power curtailment features. As for the WT system, it includes WTs and a dump load, to dissipate excess production. Lastly, a microgrid control system is required to match the power generation to the load demand and send curtailment signals to the RE systems when required.

2.2.1. Solar PV System

The PV system considered in this work consists of an array of PV modules connected to grid inverters. When there is no curtailment, the inverters use maximum power point tracking (MPPT), which convert the maximum available DC power from the PV system to AC power provided to the microgrid. The input power (P_{in}) corresponds to the DC input power produced by the PV system which is a function of the incident solar irradiance and temperature. The input DC power is also limited by the inverter's maximum AC output (P_{nom}). The relation between P_{in} and AC output power converted by the inverter (P_{out}) is given by,

$$\left(\frac{P_{in}}{P_{nom}}\right) = k_2\left(\frac{P_{out}}{P_{nom}}\right)^2 + k_1\left(\frac{P_{out}}{P_{nom}}\right) + k \quad (2)$$

Where k, k_1 and k_2 are losses coefficients obtained from the inverter efficiency characteristic curve based on tests ran by the California Energy Commission [26]. The PV system has been modelled considering the Enphase M250 Microinverter [27] and the Eclipsall NRG 60M 250M solar panel [28].

2.2.2. Wind Energy System

To ensure that the study is more realistic and applicable in a real-life scenario, the WT power system was modelled considering commercially available WTs suitable for Arctic conditions. Experts from CanmetENERGY-Ottawa developed a list of WTs fit for arctic conditions. These devices are equipped with de-icing mechanisms and components that work in extreme cold. Considering the electrical load profile of the small community, the identified WT is the Eocycle EOX S-16, rated at 25 kW [29]. To convert the wind speed measured at ground-level in the community to the wind speed at hub height of 23.8 m, taken from the data sheet, a wind speed multiplier (WSM) was calculated considering a small community with hilly surroundings. For this specific study, an average wind speed at hub height of 7.01 m/s is obtained. The WSM is implemented in the wind power system model. The WT is modelled as a set of 2nd or 3rd order equations which link the input wind speed to the power output based on the WT's power curve. Each equation has a coefficient of determination (R^2) of at least 0.99 in relation with the data points obtained along with the power curve. The set of equations and the power curve are shown in Table 1 and Figure 5, respectively. For the given wind speed profile at hub height and the power curve, 19.6% of the data points are under the WT cut-in speed of 3 m/s and 0.4% are over the WT cut-off speed of 20 m/s.

Table 1 – Equations Used to Model Wind Turbine

Wind Speed (m/s)	Power Output equation (kW)
0-3	$y = 0$
3-5	$y = 0.6657*x^2 - 2.7757*x + 2.7906$
5-7	$y = 0.6686*x^2 - 2.8709*x + 3.1783$
7-9	$y = -0.7914*x^2 + 17.449*x - 67.542$
9-11	$y = -0.7371*x^2 + 16.707*x - 65.256$
11-13	$y = -0.5486*x^2 + 12.698*x - 43.982$
13-15	$y = 0.5029*x^2 - 16.412*x + 156.78$
15-17.5	$y = 0.4104*x^3 - 19.584*x^2 + 308.9*x - 1588.2$
17.5-20	$y = 19.14$
Over 20	$y = 0$

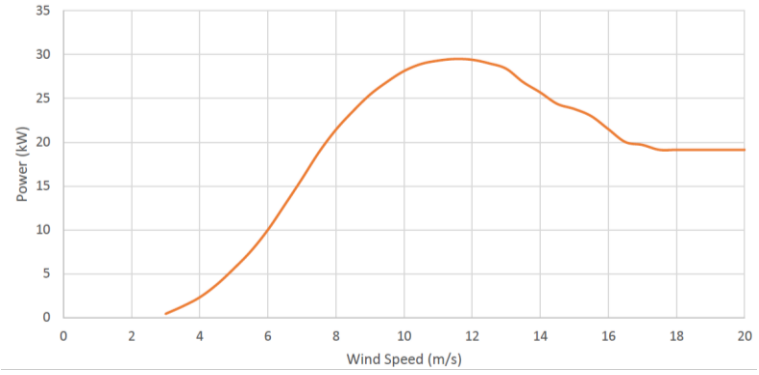

Figure 5 – EOX S-16 Power Curve

2.2.3. Diesel Generator

The diesel plant consists of two DGSs: one of 100 kW and another of 150 kW. The inputs to the DGS model are: 1) the on/off command based on a DGS dispatch strategy defined in Table 1 and 2) the required DGS power output. The DGS power depends on the instantaneous load demand and the curtailment algorithm for the PV and WT systems defined further in the text. The rated power output of the DGSs is affected by temperature and pressure [30]. P_{rated} is the maximum output power (kW) obtained when testing the device in a specific location, with an atmospheric pressure p_{rated} and a temperature T_{rated} (K). The following equation allows to obtain an adjusted rated power P_{adj}, the value used in this study, for the specific location where the DGS is installed.

$$P_{adj} = P_{rated} \cdot \frac{p_{location}}{p_{rated}} \cdot \sqrt{\frac{T_{rated}}{T_{location}}} \tag{3}$$

The rated powers of the DGSs are adjusted based on temperature and pressure values specific to the location where they are installed. Test reports for each of the gensets installed were obtained from the local utility.

These results were used to generate a normalized fuel consumption profile for both DGSs. The relation between fuel consumption, F (L/h/kW$_{rated}$) and normalized power, P is given by,

$$F = 0.0281P^2 + 0.1837P + 0.0516 \tag{4}$$

2.3. Microgrid Control System

2.3.1. Diesel Generator

The instantaneous power supplied to the grid by the diesel power plant is given by,

$$Power_{Diesel\ Plant} = Load\ Demand\ - Power_{PV+WT} \tag{5}$$

When both DGSs are on at the same time, the power output is split based on a proportion of their rated power. As the demand of the DGS power plant varies, different DGS combinations are dispatched so the DGSs operate as close as possible to their rated power which generally leads to higher efficiency. The MATLAB Stateflow toolbox is used to implement a generic DGS dispatch strategy (Table 2) which is typically used by the utility. Underloading is defined as operating a DGS under 30% of its rated power [31] and is prevented by the DGS dispatch strategy.

Table 2 – Diesel Generator Dispatch Strategy

Rated Power (kW)	Generator Combination (G1 = 100 kW, G2 = 150 kW)	Transition Criteria (kW)
100 to 150	G1 to G2	$P_{out} > 90$
150 to 100	G2 to G1	$P_{out} < 85$
150 to 250	G2 to G1 + G2	$P_{out} > 135$
250 to 150	G1 + G2 to G2	$P_{out} < 130$

DGS manufacturers [32] consider that underloading periods longer than 15 minutes should be avoided. To avoid underloading, curtailment for the RE systems is introduced.

2.3.2. Power Curtailment

Power curtailment for the PV system is first calculated considering the minimum loading requirement of the DGS. Then, if the PV output is curtailed down to zero and the minimum loading of the DGS has still not been reached, the WT output power is curtailed. This strategy is chosen because the curtailment of the selected WT requires a dump load for the excess WT generation. On the other hand, the PV curtailment can be done by controlling the inverter. For simulations with either only PV or only WTs, the algorithm is adjusted accordingly. The curtailment algorithm used in this study is presented in Table 3. When using the curtailment algorithm in the model, simulation results show that all underloading periods last less than 15 minutes.

Table 3 – Power Curtailment Algorithm

1) If Load Demand - Power WT - Power PV MPPT >= DGS Min Load Requirement: No RE curtailment. If condition is not satisfied, go to 2).
2) If Load Demand - Power WT - Power PV MPPT < DGS Min Load Requirement: Power PV is curtailed until Load Demand - Power WT - Power PV Supplied >= DGS Min Load Requirement. If condition is still not satisfied when Power PV Supplied reaches 0, go to 3).
3) After fully curtailing the PV production, curtail WT production (through dump load) until Load Demand - Power WT Supplied >= DGS Min Load Requirement.

For example, if the load demand is 100 kW and the MPPT PV production is 35 kW while the WTs produce 30 kW, the 100 kW DGS (G1) will provide the remaining 35 kW. In this case, 35 kW is higher than the minimum loading requirement of G1. Therefore, no RE curtailment is required. On the other hand, if the load demand is 40 kW and the PV and WT systems produce 20 kW and 15 kW respectively, RE curtailment will be required. In this case, the PV will first be totally curtailed to 0 kW supplied. Next, 5 kW of the WT production will be sent to the dump load while 10 kW is supplied to the grid. Lastly, the 100 kW DGS (G1) will supply the remaining 30 kW, which respects its minimum loading requirement.

2.3.3. Implementation Considerations for Real-Life Scenario

This section has the objective of making the control strategy presented in this study applicable in a real-life scenario. It details specific methods and components that could be used to apply the presented strategy to a microgrid controller. First, a measure of the total load demand of the microgrid, which is available from the meter of the DGS plant, is required. Then, DGS monitoring and control can be done using a DGS controller, such as the Kohler – SDMO APM403 [33], which allows to control and measure the power output of a DGS and to send on/off commands. To apply the curtailment algorithm to the WT and PV systems, specific devices are needed. For the PV system, inverters can be controlled to reduce the DC reference of solar panels to limit the DC power output [34]. For example, Schneider Electric CL Series inverters [35] can curtail PV output using this technique. As for a WT system, the power curtailment can be implemented with a dump load where excess power generation is sent [36]. The dump load should be rated for the maximum output

of the WT system, which is 29.5 kW by WT is this scenario. WT controllers such as the Mika-Teknik WP4100 MK II [37] allow for dump-load control.

2.3.4. Assumptions for the Analysis

The analysis done for this study focuses on energy with steady-state models. The turn-on and turn-off times and related fuel consumption of gensets are neglected. Inverters are assumed to be identical with similar inputs resulting in similar output power production for each unit.

2.4. MATLAB Simulink Model Representation

This section presents MATLAB Simulink model based on the elements and control systems defined in sections 2.2 and 2.3. First, Figure 6 presents the diesel genset model.

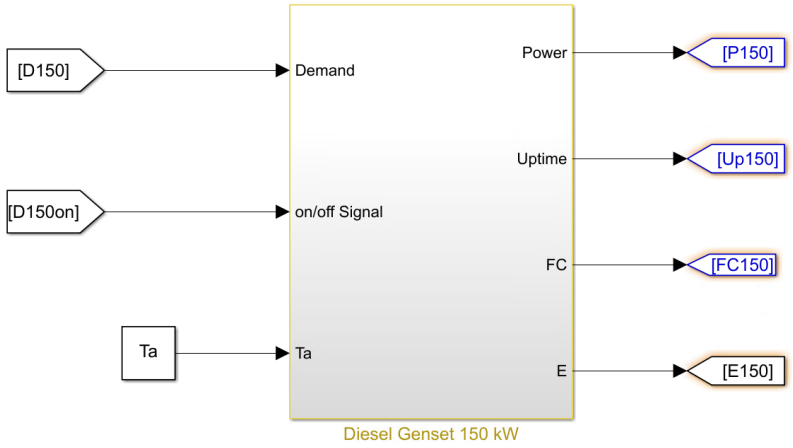

Figure 6 – Diesel Generator Matlab Simulink Model

The genset object is part of the PVToolbox [24] and represents the behaviour of the diesel generator based on a fuel curve obtained from the utility (equation 4). The input values to the block are the demand to be supplied by the DGS (D150) after calculating RE curtailment, a turn-on/off signal (D150on) and the ambient temperature (Ta). The output values of this block include its instantaneous power generated (P150), its cumulative runtime (Up150), its total fuel consumption (FC150) and its cumulative energy produced (E150). Then, Figure 7 shows the PV and WT Curtailment Controller model.

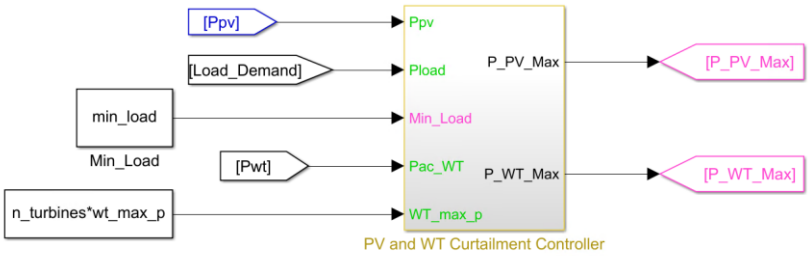

Figure 7 – PV and WT Curtailment Controller MATLAB Simulink Model

This block contains a MATLAB function block that calculates the maximum allowed power for the PV (P_PV_Max) and WT (P_WT_Max) system, based on the curtailment algorithm described in Table 3. The required inputs are the power generated by the PV and WT systems (Pv and Pwt) for given meteorological conditions, the load demand (Load_Demand) and the minimum loading requirement of the DGS (min_load). Next, Figure 8 presents the PV System model.

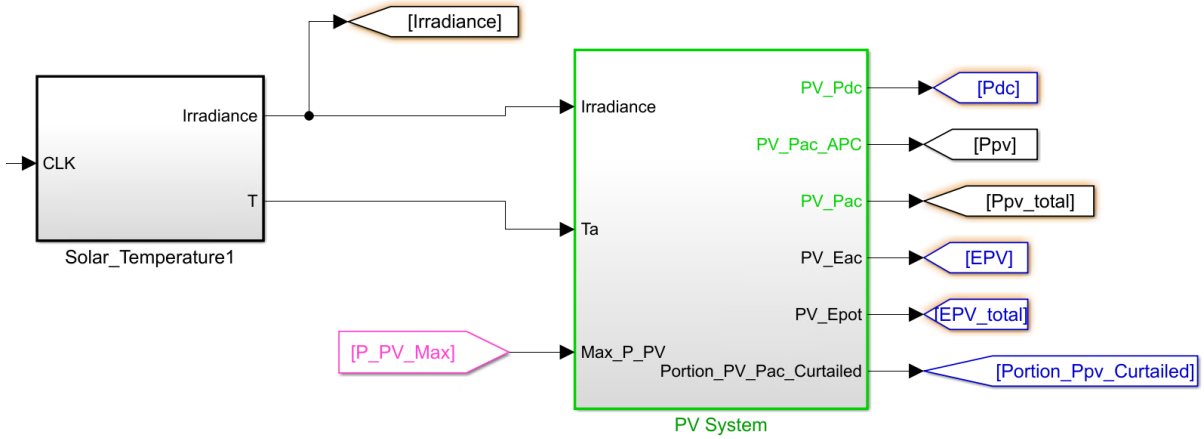

Figure 8 – PV System MATLAB Simulink Model

This system is modelled based on a PV at MPPT object from PVToolbox [24] and GridInverter block to convert the DC power output of the PV panels to AC. It takes solar irradiance (Irradiance) and the ambient temperature (Ta) as inputs, as mentioned in section 2.1.2. The block calculates both the total potential PV production (Ppv_total and EPV_total) and what is actually produced (Ppv and EPV) considering the curtailment algorithm (Figure 7) and the associated P_PV_Max. Therefore, the block can calculate what amount of the production is curtailed. Lastly, CLK represents the clock signal of the simulation, which is used to access specific data (irradiance, wind speed, …) at a given timestamp. Figure 9 shows the WT system model.

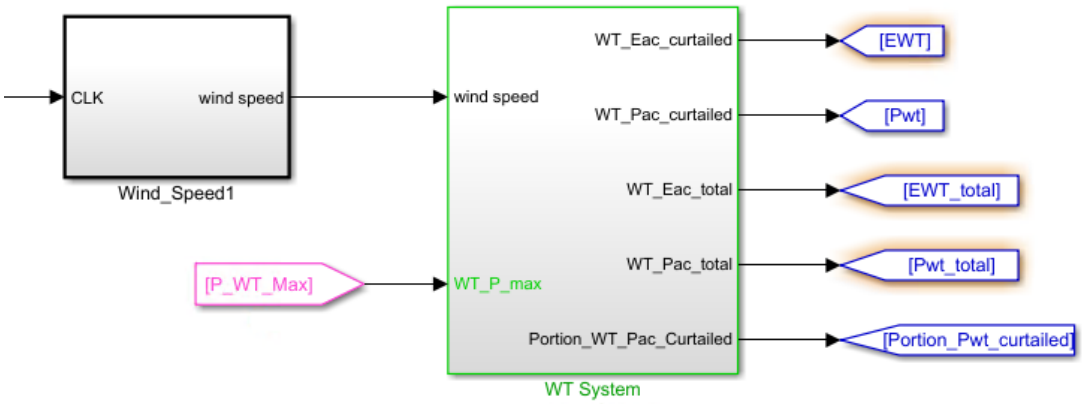

Figure 9 – WT System MATLAB Simulink Model

The WT system block contains a MATLAB function block which calculates the output power based on the wind speed, as defined in Table 1. The block takes wind speed data as an input, as defined in section 2.1.2. It also requires the maximum allowed power supplied by the WT system (P_WT_Max) Similarly to the PV system block, both the total potential WT production (Pwt_total and EWT_total) and the real production (Pwt and EWT), based on the curtailment algorithm, are calculated. Lastly, Figure 10 presents the DGS dispatch strategy model.

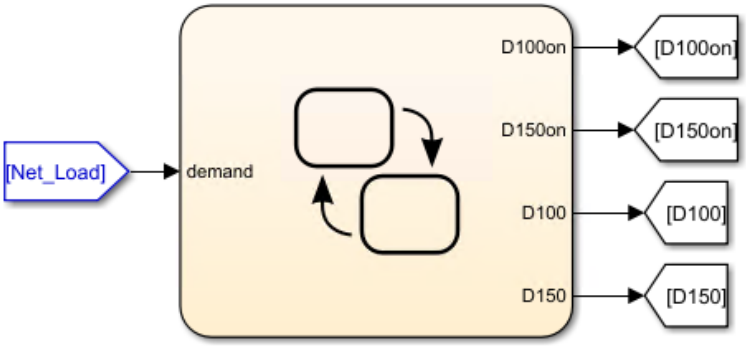

Figure 10 – Simulink Stateflow Block for Diesel Genset Dispatch Strategy

This block represents the logic used to dispatch the different diesel generators based on the load demand and allowed renewable energy production. It follows the limits defined in Table 2. Net_Load represents the demand to be met by the DGS considering the instantaneous RE production and curtailment, if required. D100on and D150on represent the turn-on/off signals sent to the DGSs while D100 and D150 dispatch the power to be produced by the DGSs.

Chapter 3 - Renewable Energy Low Penetration Utilization Analysis

In this chapter, different RE configurations are tested, using the MATLAB Simulink model presented in the earlier section, to assess their potential to reduce the fuel consumption and GHG emissions of the community. This part of the study is labelled as a low penetration of RE analysis since no storage or load-side management is considered in the following scenarios. The simulation scenarios consider the following combinations of power generation systems: 1) DGSs + PV, 2) DGSs + WTs and 3) DGSs + PV + WTs. The results are presented in the following subsections.

To quantify how the RE production matches the load demand of the microgrid, the correlation between these datasets is studied. The Pearson Correlation Coefficient (PCC) is a number between –1 and 1 that measures the strength and direction of the relationship between two variables. The PCC is first calculated between the instantaneous power values of the RE production, before curtailment, and the load demand throughout the year to evaluate their overall match. For example, if the load demand were concentrated during the daytime and peaked around noon, it would have a highly positive correlation with PV production. However, since the PCC does not consider the magnitude of the datasets, it cannot identify whether periods of high production and high demand are correlated throughout the year. Therefore, to assess whether the RE production and the load demand tend to vary similarly over longer periods of time, the PCC is calculated for datasets containing the monthly amounts of energy provided by the RE systems and the one required by the microgrid.

3.1. Diesel-PV Original Scenario

The first scenario considers a Diesel-PV power plant. The simulations are executed with PV arrays ranging from 2.5 to 200 kW, in steps of 2.5 kW. The summary of the simulation results for the Diesel-PV system is presented in Table 4. The addition of PV to the diesel plant yields significant fuel savings and PV penetration. However, when adding more and more PV, the savings, for each additional 2.5 kW of PV, get smaller due to the important increase in curtailment of the RE system. Then, Figure 11 presents the monthly normalized energy demand of the community compared to the PV production. It shows that, overall, the PV production tends to increase while the energy demand of the community reduces during the summer and vice versa for the winter months.

Table 4 – Simulation Results for Diesel-PV Configuration

PV Installed (kW)	2.5 – 200
PV Penetration (%)	0.5 – 22
PV Curtailment (%)	0 – 50.5
Fuel Consumption Reduction (%)	0.5 – 18
Load vs. PV Power Correlation	+0.17
Load vs. PV Monthly Energy Correlation	-0.40

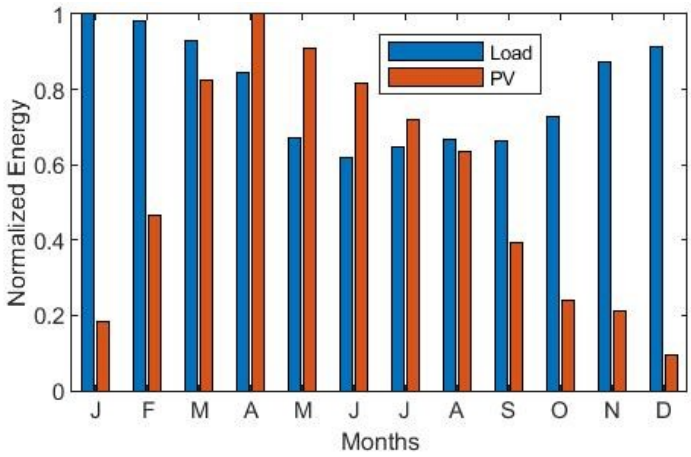

Figure 11 – Monthly Normalized Energy Demand vs. PV Production

First, there is close to no correlation between the minute-level PV production and the load demand. However, there is a substantial negative correlation between the monthly PV energy produced and the monthly energy required by the community. That result is confirmed when observing Figure 11. Next, Figure 12 shows the monthly PV energy supplied and curtailed for a PV system of 120 kW. The negative correlation between the monthly PV energy produced and energy required by the community leads to high PV curtailment, mostly during the summer (Table 5). In this example, the annual PV curtailment is 31%.

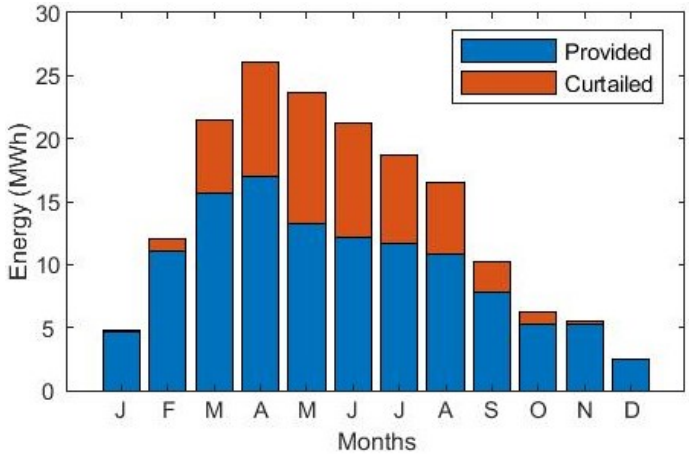

Figure 12 – Monthly PV Energy Supplied and Curtailed for 120 kW

Table 5 – 120 kW PV – Monthly Percentage of PV Production Curtailed (%)

J	F	M	A	M	J	J	A	S	O	N	D
2.5	8.2	27.1	34.8	43.8	43.0	37.3	34.7	23.1	15.2	5.7	0

Next, Figure 13 and Table 6 show the portion of energy supplied by the PV system and the diesel power plant for the same configuration of 120 kW of PV. The yearly fuel savings associated to the PV system are 28 kL (15%).

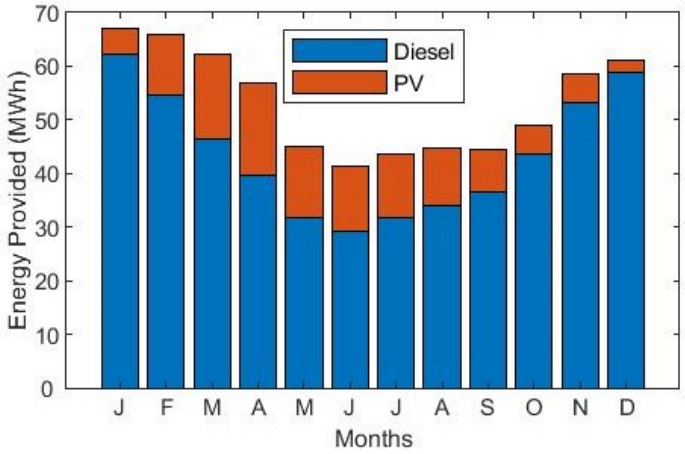

Figure 13 – Monthly Portion of Energy Supplied for DGS + 120 kW of PV

Table 6 – 120 kW of PV – Monthly Percentage of Energy Supplied by PV

J	F	M	A	M	J	J	A	S	O	N	D
7.0	16.9	25.2	29.9	29.5	29.2	27.0	24.1	17.6	10.8	8.9	4.0

As expected, the PV system provides more energy to the grid during the sunnier months of the year and much less from October to January.

3.2. Introduction of WTs to the Study

The second scenario considers a Diesel-Wind power plant. The simulations are executed with 1 to 3 WTs, each rated at 25 kW. The simulation results for the Diesel-PV system is presented in Table 7.

Table 7 – Simulation Results for Diesel-Wind Configuration

Number of WTs (25 kW each)	1 – 3
WT Penetration (%)	18 – 36
WT Curtailment (%)	4 – 35
Fuel Consumption Reduction (%)	15 – 29
Load vs. WT Power Correlation	+0.10
Load vs. WT Monthly Energy Correlation	+0.67

Once again, there is no clear correlation between the instantaneous power produced by the WT and the load demand of the community. However, when considering longer periods of time, the correlation is much higher. Indeed, there is a high positive correlation between the monthly WT energy produced and the energy required by the community. This leads to increases in fuel savings and RE penetration when compared to the PV system while also maintaining the curtailment much lower. Then, Figure 14 presents the monthly normalized energy demand of the community compared to the WT production.

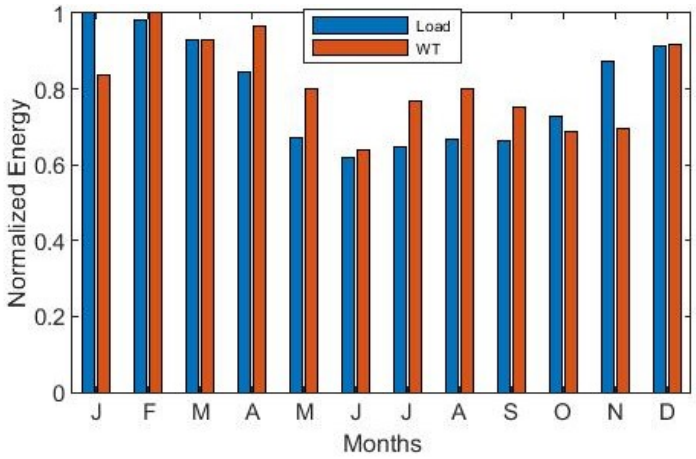

Figure 14 – Monthly Normalized Energy Demand vs. WT Production

It indeed shows a clear correlation between the energy demand and the energy produced by the WT system unlike for the PV system. Next, Figure 15 and Table 8 present the monthly energy supplied and curtailed for a power plant which included one WT. In this example, the fuel savings are the same as for with 120 kW of PV (15%). However, the WT production is curtailed slightly under 4% in this case as compared to 31% in the previous case.

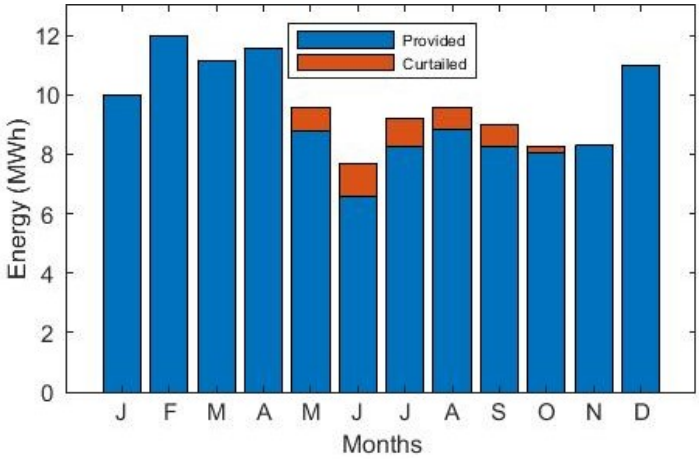

Figure 15 – Monthly WT Energy Supplied and Curtailed for 1 WT

Table 8 - Monthly Percentage of WT Production Curtailed (%)

J	F	M	A	M	J	J	A	S	O	N	D
0	0	0	0.2	8.3	14.4	9.9	7.7	7.9	2.1	0.2	0.1

For a single WT, there is close to no curtailment during the months of November to April, when the load demand is at its highest. Lastly, Figure 16 and Table 9 present the detailed monthly amount of energy provided by the WT and the diesel power plant for the same configuration.

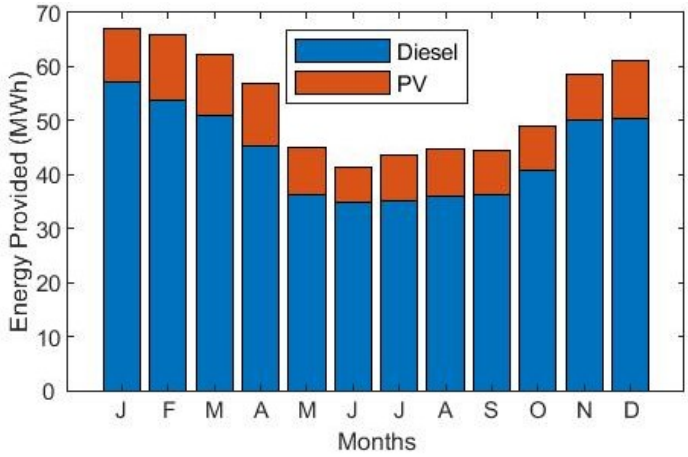

Figure 16 – Monthly Portion of Energy Supplied for DGS + 120 kW of PV

Table 9 - Monthly Percentage of Total Energy Provided by 1 WT (%)

J	F	M	A	M	J	J	A	S	O	N	D
15.8	18.4	17.2	19.7	19.2	15.0	18.8	20.1	19.1	17.3	14.7	20.4

Unlike for the PV system, the WT provides an even portion of energy to the grid throughout the year. On a yearly basis, the 25 kW WT provides 17.6% of the total energy required for the community.

3.3. Combining PV With WTs

Lastly, the third scenario considers a Diesel-PV-Wind power plant, with PV ranging from 2.5 to 200 kW alongside 1 to 3 WTs. The summary of the simulation results are shown in Table 10. When combining PV with WTs, PV is curtailed first, As mentioned in section 2.3.2. The WTs are only curtailed when the PV is totally curtailed (0 kW supplied). Therefore, the curtailment results for WTs are the same with or without PV systems.

Table 10 – Simulation Results for Diesel-PV-Wind Configuration

PV Installed (kW)	2.5 – 200
Number of WTs	1 – 3
Total RE Penetration (%)	18 – 44
PV Curtailment (%)	4 – 80
WT Curtailment (%)	4 – 35
Fuel Consumption Reduction (%)	16 – 36
Load vs. RE Monthly Energy Correlation	+0.65 – -0,33

Combining both sources of RE allows to increase penetration and fuel savings when compared to scenarios with only one source of RE. However, the same issue resurfaces when adding more PV; the correlation between the energy demand and the RE production decreases and the curtailment increases, mostly during the summer months. This phenomenon can be shown in Figure 17, which presents the monthly PV energy provided and curtailed for different scenarios with one WT and PV arrays of 50, 100 and 150 kW. The dark bars represent energy supplied while the light ones show energy curtailed. The sum of both bars represents the monthly energy produced by the PV

system considering MPPT. The PV production and curtailment increases for warmer months when there are more peak-sun hours (Figure 2), which also corresponds to the time of the year where the load is at its lowest (Figure 1). This leads to a significant PV curtailment for those periods. For example, the PV curtailment for the month of May is 34%, 57% and 69% for the three PV capacities. Furthermore, since the PV curtailment is calculated first, considering the load demand and the WT production, additional WTs would also lead to higher PV curtailment.

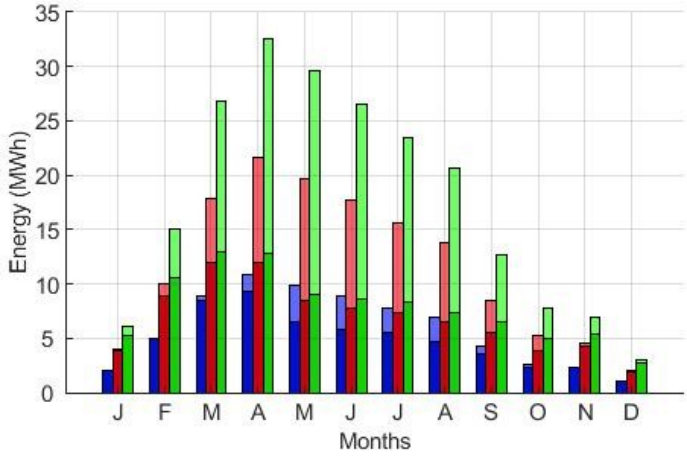

Figure 17 – Monthly PV Provided and Curtailed for Scenarios with one WT + 50 (Blue), 100 (Red) and 150 (Green) kW PV - Optimal South47

Then, Figure 18 shows the annual fuel consumption of the diesel power plant. When observing the slope of the different curves, which correspond to the addition of more PV, and the jump between the curves, which correspond to adding more WTs, one can note that the most significant reductions in fuel consumption occur at lower PV capacities and with the first wind turbine added to the system. When adding more RE, the fuel savings increase, but the gain from each additional RE equipment installed gets smaller. This is first related to the decrease in fuel efficiency of the DGSs (Figure 19) which are forced to operate further from their rated power and maximum efficiency. It is also related to the increase in curtailment. Since the system curtails the PV system first, the WT curtailment remains the same as in the Diesel-WT configuration. For 1 to 3 WTs, the curtailment is 4%, 18% and 35%. However, the PV curtailment is increased, as shown in Figure 20. Next, Figure 21 shows the combined RE curtailment for configurations with PV and WTs. Lastly, Figure 22 presents the penetration of RE which is also affected by the RE curtailment. In this setting, WTs are much more effective in terms of energy provided by kW installed than PV panels.

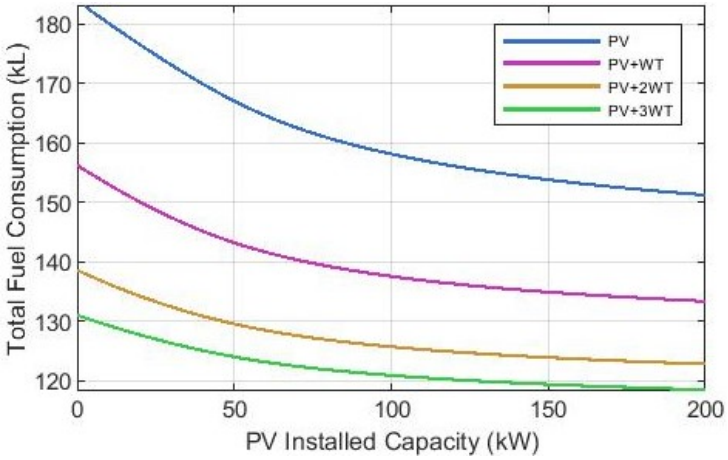

Figure 18 – Annual Diesel Fuel Consumption (kL) - Optimal South

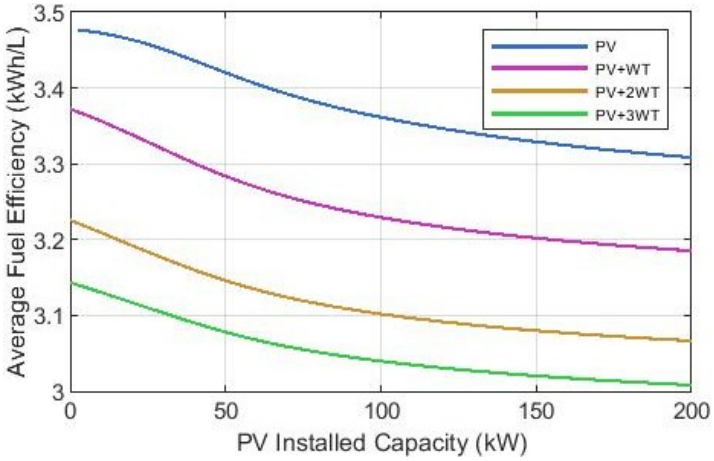

Figure 19 – Annual Fuel Efficiency (kWh/L) – Optimal South

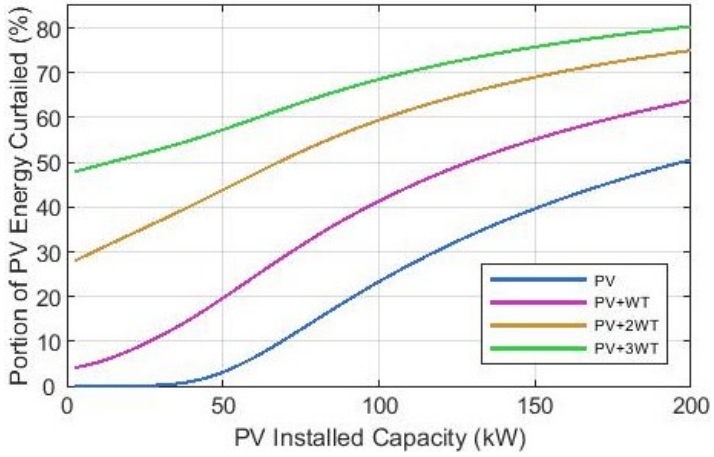

Figure 20 – Annual Portion of PV Energy Curtailed (%) - Optimal South

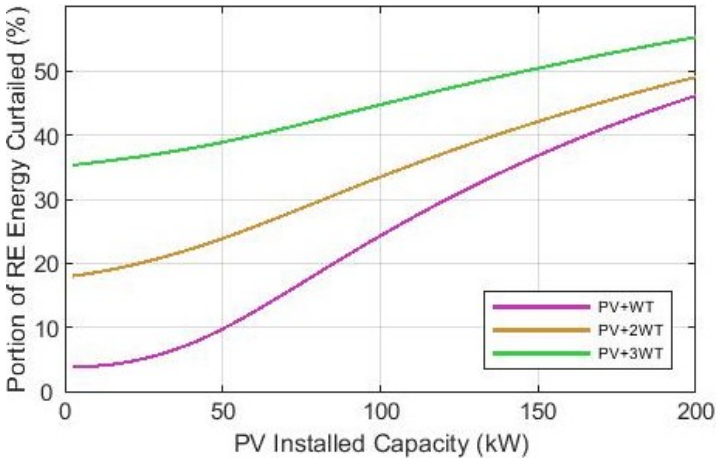

Figure 21 – Annual Portion of RE Energy Curtailed (%) - Optimal South

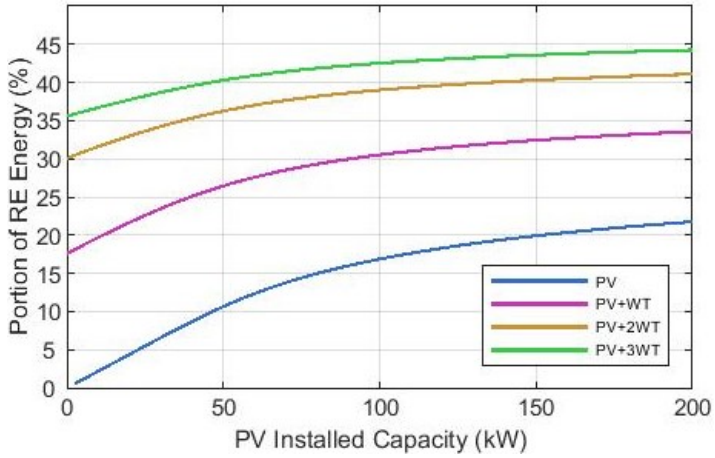

Figure 22 – Annual Portion of Energy Provided by RE (%) - Optimal South

When combining PV and WTs, the fuel consumption is reduced compared to the scenario with WT only. However, when increasing the number of WTs, the curtailment for both sources of RE increases significantly, which makes these systems less cost-effective. The PV curtailment is at least 4%, 28% and 48% when PV is combined with one to three WTs.

Consequently, different methods are investigated to increase the match between the energy demand and the PV production. Since there is no storage considered in this part of the study, the objective is to match the instantaneous RE production with the load demand to increase the PV penetration and limit curtailment thus increasing the fuel savings.

3.4. Considerations to Improve the Performance of the PV System

3.4.1. Panel Tilt to Maximize Winter Production

To increase the PV penetration during winter months, when there is little PV curtailment due to the high load and low solar irradiance, a new panel tilt of 76.1° (latitude + 15°) which maximizes winter production [38] is considered. The incident Winter South (WS) profile for the community, obtained with PVLIB Python, is shown in Figure 23. It has a peak of 1110 W/m^2 in May (3% less than OS), an average of 150 W/m^2 (same as OS) and a winter mean 116 W/m^2 (9% more than OS).

Figure 24, which presents the monthly PV production of the OS and WS scenarios without curtailment for 100 kW installed, shows that the WS configuration produces more PV energy than the OS one from October to March. Therefore, the two-tilt (TT) scenario, using the winter tilt from October to March and the optimal tilt from April to September is considered. Overall, it produces 3% more energy throughout the year than a system of the same size using the OS configuration. With this combined irradiance profile, the PCC shows an improvement in correlation between the load and the PV production. For monthly energy, the correlation is -0.36 vs -0.40 for the OS scenario.

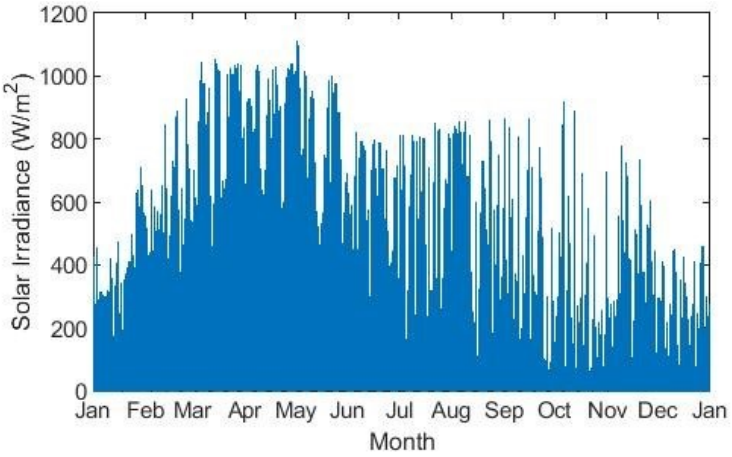

Figure 23 – Yearly Irradiance Profile - Winter Tilt (76.1°)

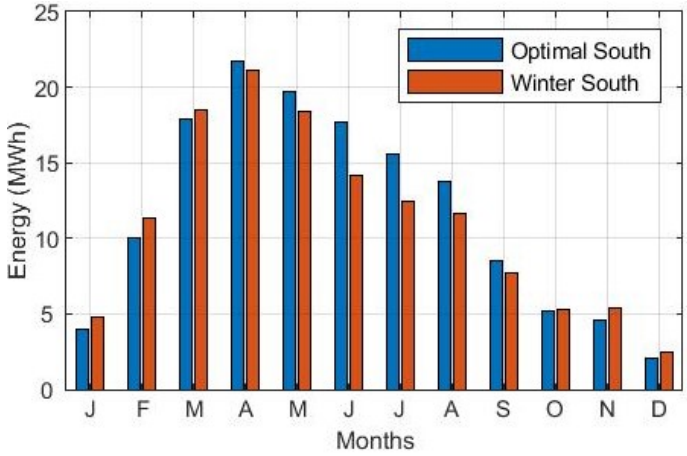

Figure 24 – Total Monthly PV Production – Optimal South vs. Winter South – 100 kW

The TT scenario simulation results are compared to the OS scenario and shown in Table 11, for RE configurations with PV only.

Table 11 – Simulation Results for Diesel-PV Configuration Comparing the OS and TT Configurations

Results	Optimal South	Two-Tilt
Installed PV Capacity (kW)	2.5 - 200	2.5 - 200
PV Penetration (%)	0.5 – 22.0	0.6 – 22.1
PV Curtailment (%)	0 – 50.5	0 – 51.2
Fuel Consumption Reduction (%)	0.5 – 17.7	0.5 – 18.0

The results for both these configurations are almost identical. Even though the TT PV configuration produces 3% more energy than the OS one, the increase in curtailment limits the gain in fuel savings to only 0.5 kL more for the TT configuration in the best-case scenario (200 kW PV without WTs). With that in mind, the TT scenario is put aside for the rest of the study since added equipment and O&M costs associated with being able to change the panel tilt are not deemed worthy of such small gains in fuel savings.

3.4.2. East-West Configuration

Another potential solution to reduce the PV curtailment and increase its penetration is to modify the panel azimuth. One possibility would be to consider a scenario where half of the panels are oriented east, and the other half is oriented west with an optimal tilt. The east-facing panels produce more energy during the morning while the west-facing ones produce more energy during the afternoon which allows the plant to produce a more continuous output throughout the day instead of a peak around noon [39]. A PV panel oriented either east or west does not supply as much energy as one would if it were oriented south. However, since the production of east and west-facing panels is complementary and more continuous, they can be combined in a configuration which requires a lower inverter rating than another where all the PV panels are south-facing. In Old Crow, Yukon, a solar farm using an east-west (E-W) PV configuration with 940 kW of panels (DC) and 480 kW of inverter capacity (kW) was launched in 2021 [40], [41].

In the earlier sections, for the OS, WS and TT PV scenarios, the Enphase M250 microinverter was considered. These devices are small, and one is required for every panel. These provide flexibility since they all control the MPPT point of their associated PV panel. On the other hand, a string inverter is a different type of DC-AC converter, with one or multiple strings of panels attached to it. Some modern string inverters are equipped with multiple DC-DC converters and MPPT controllers allowing to control different strings independently. When connecting multiple panels with different orientations or tilts to a single MPPT controller, the panel which produces the least amount of power pulls down the performance of all the panels of the string. This phenomenon is called panel mismatch. The same issue can happen when one panel of a string is shaded or covered. Therefore, string inverters with at least two MPPT controllers, one for the east-facing string and another for the west-facing one, are required for an E-W PV configuration [39], [42], [43].

Next, multiple MPPT inverters that are available in Canada and can operate under Arctic conditions, down to temperatures of – 40°C, are identified and compared to the M250 Microinverter in Table 12.

Table 12 – Inverter Characteristics and Cost

Inverter Model	AC Power Rating (W_{AC})	MPPT Inputs	Cost ($/$W_{AC}$) [44], [45]
Enphase M250 Microinverter [27]	250	1	0.82
SMA Sunny Boy 5.0 US [46]	5000	3	0.46
Fronius Primo 5.0-1 [47]	5000	2	0.52

The most noticeable element is that the identified string inverters, equipped with multiple MPPT controllers, are much cheaper than the microinverter considered in the first part of the study. Considering that an E-W PV configuration requires a lower inverter capacity than an OS one, and that the string inverters equipped with multiple MPPT controllers are cheaper than the

microinverters considered earlier in the study, this would suggest that, for a given financial investment, more PV panels can be installed for the E-W than for the OS one. Therefore, even though each panel produces less energy in an E-W configuration, it could potentially be a viable technical and financial solution. Obviously, in a design scenario for a remote Arctic community, a further assessment of the different configurations would be required. For example, the shipping costs associated to sending solar equipment to the Arctic should be considered.

Now, let us focus on the technical aspects of the E-W configuration. First, using Python PVLIB, the yearly PV potential of the community, measured in kWh/m^2, was generated for multiple tilt angles and azimuths to identify which tilt to choose for the E-W configuration. That methodology is the same one which was used to generate the PV profiles for the OS or WS configurations (section 2.1.2). Figure 25 presents the obtained results. Image a) shows the potential for all the possible azimuth and tilt angles while images b) and c) focus on the PV potential for azimuths close to 90° (East) and 270° (West).

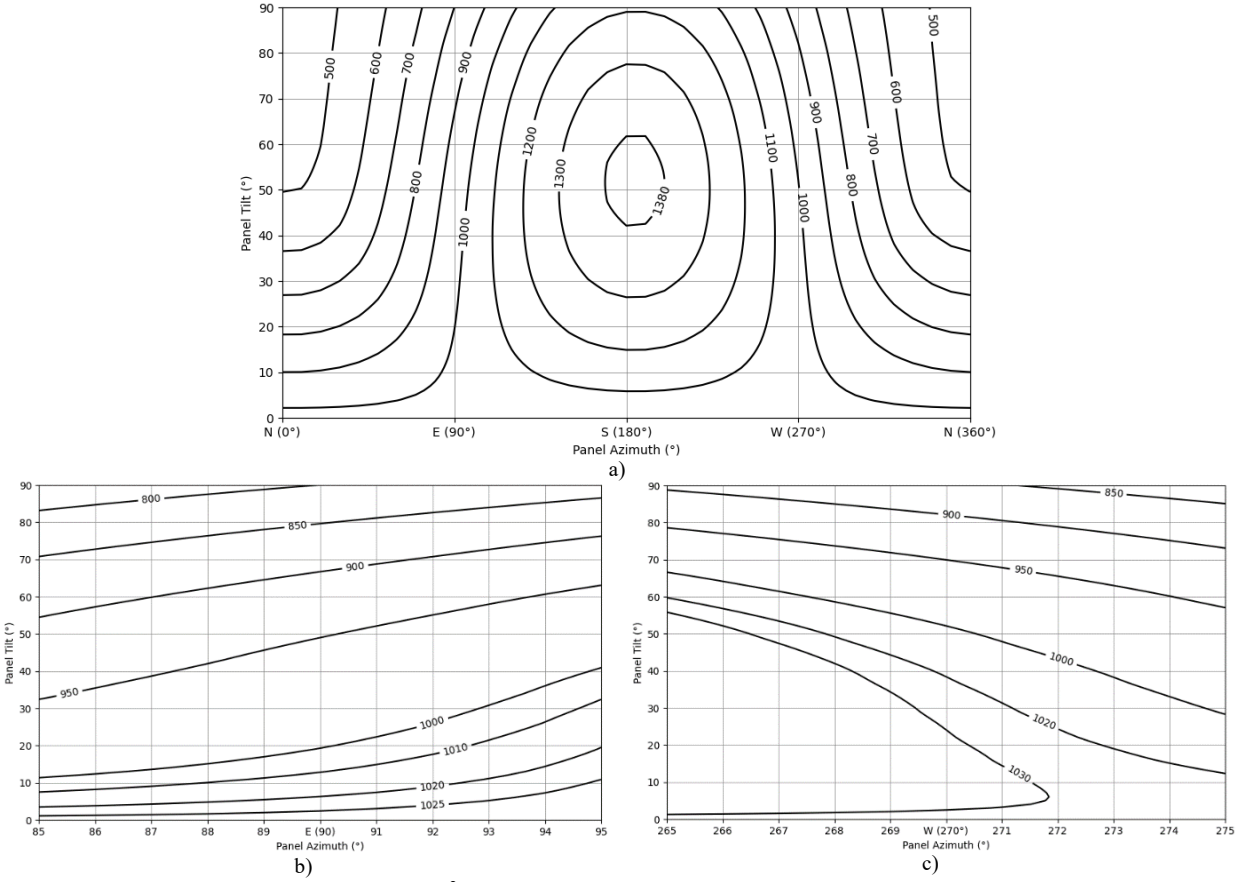

Figure 25 – Solar Insolation Potential (kWh/m^2) of the Community – a) Overall Potential, b) East-Facing Potential and c) West-Facing Potential

From that figure, one can clearly notice that east- and west-facing panels have a higher potential at small tilts, where they are almost horizontal. However, for an E-W configuration, the potential reduces slowly. For example, the average potential of an E-W configuration is 1027 kWh/m^2 at a 0° tilt and 978 kWh/m^2 at a 48.8°, when considering the same tilt as the one used for the OS. This corresponds to a reduction of less than 5%. This slow decrease in potential when increasing the tilt of the panels must be kept in mind since the objective is to obtain a continuous production

throughout the day which could reduce the inverter capacity required. Unfortunately, with PV panels being almost horizontal, the solar production will remain concentrated in the middle of the day. Therefore, different panel tilts will be considered in the simulation to assess their effect of the obtained PV penetration, curtailment, and fuel savings as well as the required inverter capacity. First, Table 13 presents the maximum combined DC power output of an east-facing and a west-facing PV panel for different tilts. The power correlation and the monthly energy correlation are also presented for the same tilts. These correlation values are obtained when simulating the total production of the PV panels considering an E-W configuration.

Table 13 – East-West PV Configurations Statistics for Different Tilts

PV Tilt (°)	Peak Combined DC Output (W)	Power Correlation	Monthly Energy Correlation
5	411	0.0109	-0.6592
10	409	0.0116	-0.6563
15	405	0.0127	-0.6516
20	399	0.0136	-0.6452
25	392	0.0145	-0.6371
30	382	0.0152	-0.6275
35	371	0.0158	-0.6163
40	358	0.0164	-0.6037
45	343	0.0171	-0.5897
50	327	0.0178	-0.5746
55	312	0.0187	-0.5582

As mentioned above, when increasing the tilt of the PV panels, the east-facing panel will produce more in the morning while the west-facing one will produce more in the afternoon. This therefore results in a lower peak combined DC output of the panels. Also, there is no power correlation between the PV production and the load demand and the monthly energy correlation is significantly negative and lower than it was for the OS scenario (-0.40). However, the correlation results tend to improve with higher PV tilts.

Next, simulations are run with all the aforementioned PV tilts for total installed DC capacities of 25, 50, 75 and 100 kW. These results are detailed in Table 14.

Table 14 – Detailed PV Simulation Results - East-West Configuration

PV Installed Capacity (kW)	PV Tilt (°)	PV Penetration (%)	PV Curtailment (%)	Fuel Savings (kL)	Fuel Savings (%)
25	**5**	**3.99**	**0.06**	**6.41**	**3.49**
	10	3.98	0.06	6.40	3.48
	15	3.97	0.05	6.39	3.48
	20	3.95	0.05	6.38	3.47
	25	3.94	0.04	6.37	3.46
	30	3.92	0.04	6.35	3.45
	35	3.90	0.05	6.33	3.44
	40	3.88	0.05	6.30	3.43
	45	3.85	0.05	6.27	3.41
	50	3.81	0.06	6.23	3.39
	55	3.77	0.07	6.17	3.35
50	**5**	**7.84**	**1.76**	**12.19**	**6.63**
	10	7.83	1.71	12.17	6.62

	15	7.81	1.62	12.16	6.61
	20	7.79	1.49	12.15	6.61
	25	7.77	1.36	12.14	6.60
	30	7.75	1.24	12.12	6.59
	35	7.71	1.16	12.10	6.58
	40	7.67	1.11	12.06	6.56
	45	7.62	1.09	11.99	6.52
	50	7.55	1.10	11.91	6.48
	55	7.47	1.11	11.79	6.41
75	5	11.02	7.95	16.82	9.15
	10	11.02	7.80	16.82	9.14
	15	11.01	7.50	16.83	9.15
	20	11.02	7.07	16.87	9.17
	25	11.04	6.58	16.91	9.20
	30	11.05	6.06	16.96	9.22
	35	**11.06**	**5.55**	**16.98**	**9.23**
	40	11.04	5.10	16.98	9.24
	45	11.01	4.70	16.95	9.22
	50	10.95	4.40	16.88	9.18
	55	10.85	4.19	16.75	9.11
100	5	13.37	16.26	20.21	10.99
	10	13.37	16.04	20.23	11.00
	15	13.40	15.59	20.29	11.03
	20	13.45	14.96	20.38	11.08
	25	13.52	14.20	20.50	11.15
	30	13.59	13.37	20.62	11.21
	35	13.65	12.53	20.73	11.27
	40	13.70	11.72	20.80	11.31
	45	**13.71**	**10.97**	**20.83**	**11.33**
	50	13.69	10.32	20.82	11.32
	55	13.63	9.75	20.74	11.28

For installed capacities of 25 and 50 kW, the best results in terms of fuel savings and PV penetration are obtained with tilts of 5° since the curtailment remains low for all PV tilts. However, for 75 and 100 kW, the suggested tilts are 35° and 45°, respectively. When installing more PV, the curtailment starts to influence the overall performance of the system, and higher tilts, which provide a more continuous production throughout the day, provide better results. This would suggest that, when the objective is to maximize the penetration and the fuel savings, the higher tilts are a better fit.

Let us now compare the results obtained in this section to the ones obtained for the OS scenario. First, simulations were rerun for 100 kW of south-facing PV (OS). Then, considering a 2:1 DC/AC configuration as an objective, simulations were run to obtain the same fuel savings as with 100 kW of installed PV considering the OS scenario. The identified configuration, which yielded the same fuel savings, consists of 147 kW of installed PV panels (DC), at a 50° tilt. For that configuration, the inverter capacity is 75 kW, which is the closest possible value to a 2:1 DC:AC ratio when considering the inverters presented in Table 12. The simulation results of these two configurations are presented in Table 15.

Table 15 – Simulation Results Comparison - OS vs. E-W

PV Configuration	DC Capacity (kW)	AC Capacity (kW)	Total Energy Produced (MWh)	PV Penetration (%)	PV Curtailment (%)	Fuel Savings (kL)
Optimal South	100	100	140.8	16.9	23.5	25.7
East-West (50°)	147	75	142.4	17.1	23.0	25.7

Figure 26 presents the average daily PV production profile for both configurations with 100 kW (OS) and 147 kW (E-W) of installed panels.

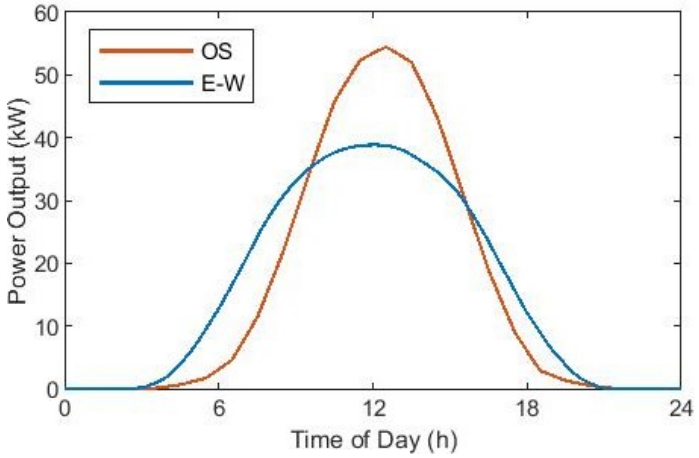

Figure 26 – Average Daily PV Production Profile

As expected, the production profile of the OS configuration is concentrated around noon while the E-W still peaks around noon but is much more spread out throughout the day and produces more during the morning and evening. It is also interesting to note that, even though the DC installed capacity of the OS configuration is about 40 kW lower than it is for the E-W one, its peak average production is still higher. To further analyze the performance of those two configurations, their detailed monthly PV energy production, penetration and curtailment are presented graphically in Figure 27 and then numerically in Table 16.

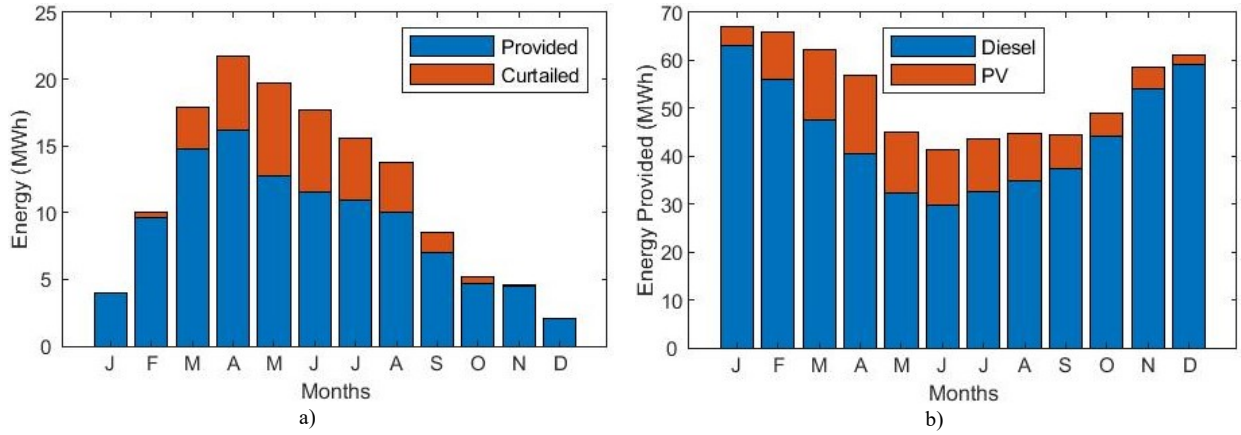

a) b)

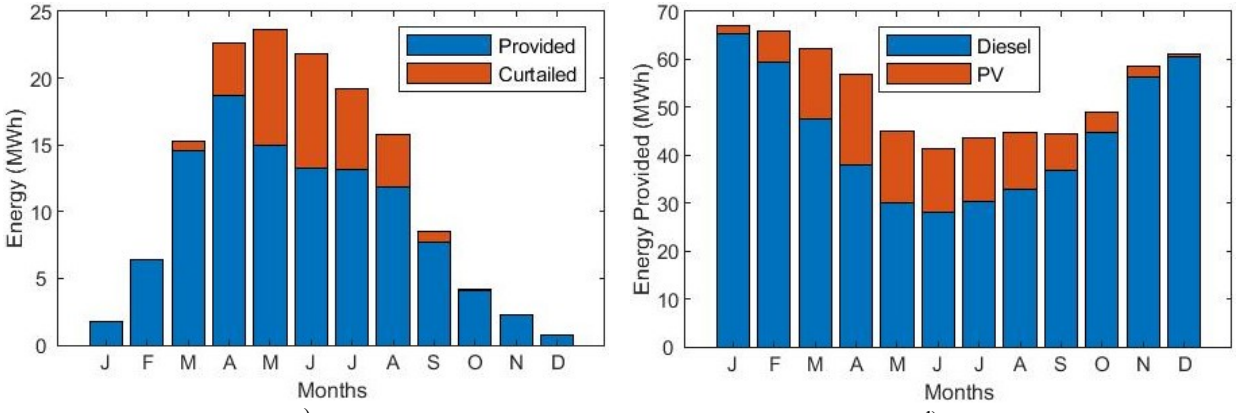

Figure 27 – Monthly PV Simulation Results - a) PV Production (OS), b) PV Penetration (OS), c) PV Production (E-W) and d) PV Penetration (E-W)

Table 16 – Monthly Percentage of PV Production Curtailed (%)

Optimal South – 100 kW											
J	**F**	**M**	**A**	**M**	**J**	**J**	**A**	**S**	**O**	**N**	**D**
0.6	4.1	17.7	25.5	35.3	35.0	30.0	27.4	17.4	10.3	2.4	0
East-West 50° – 147 kW DC / 75 kW AC											
J	**F**	**M**	**A**	**M**	**J**	**J**	**A**	**S**	**O**	**N**	**D**
0	0	4.5	17.5	36.7	39.3	31.7	25.0	9.4	0.5	0	0

Table 17 – 100 kW of PV – Monthly Percentage of PV Penetration

Optimal South – 100 kW											
J	**F**	**M**	**A**	**M**	**J**	**J**	**A**	**S**	**O**	**N**	**D**
6.0	14.7	23.7	28.4	28.3	27.8	25.1	22.4	15.8	9.5	7.7	3.3
East-West 50° – 147 kW DC / 75 kW AC											
J	**F**	**M**	**A**	**M**	**J**	**J**	**A**	**S**	**O**	**N**	**D**
2.7	9.7	23.4	32.9	33.2	31.9	30.2	26.4	17.4	8.5	4.0	1.3

The detailed results show that, overall, these two configurations provide the same amount of fuel savings as well as similar curtailment values. Also, the PV production of the E-W configuration is much more concentrated in the summer months when the load demand is lower. However, the E-W configuration reduces the curtailment during summer months when compared to an OS equivalent with similar monthly energy produced. Indeed, when comparing the E-W configuration with the one presented in section 3.1, with an OS scenario and 120 kW of PV (Figure 12), the energy these two produce is similar, but the curtailment is much lower for E-W PV (Table 5). More specifically, their curtailment is 43.8% (OS) vs. 33.2% (E-W) in May, 43.0% vs. 31.9% in June and 37.3% vs. 30.2% in July while the differences in their monthly PV energy produced stay within 2%.

Lastly, these results show that the E-W PV configuration could be a relevant solution for a low-penetration regime of RE integration in a remote community due to the more continuous PV production as well as the higher ratio between the DC and AC capacities, which reduces the amount of inverters required. However, these two configurations are hard to compare in the context of this study. A more thorough techno financial comparison of the two proposed scenarios would be required to accurately identify the savings associated with reducing the inverter AC capacity and how many additional panels could it fund. Moreover, the difference in the configuration would also

influence the O&M costs of the system as well as the shipping costs. Given that uncertainty, the E-W configuration is not considered for the next steps of the study.

3.4.3. Modified Orientation

Another potential solution to reduce the PV curtailment and increase its penetration is to slightly modify the panel orientation. Here, the idea is to install the PV panels at a different azimuth than true south to try to increase the match between PV production and the load demand. For a load demand that is concentrated in the AM, rotating the PV panels slightly east of south would increase the correlation between the PV production and the demand. Using the same logic, orienting the panel slightly west of south would match better with a load demand which peaks in the afternoon. Therefore, the yearly load demand of the community (Figure 1) was analyzed to obtain the average hourly-aggregated load demand of the community. This data is shown in Figure 28 and represents an average representative daily load profile of the microgrid.

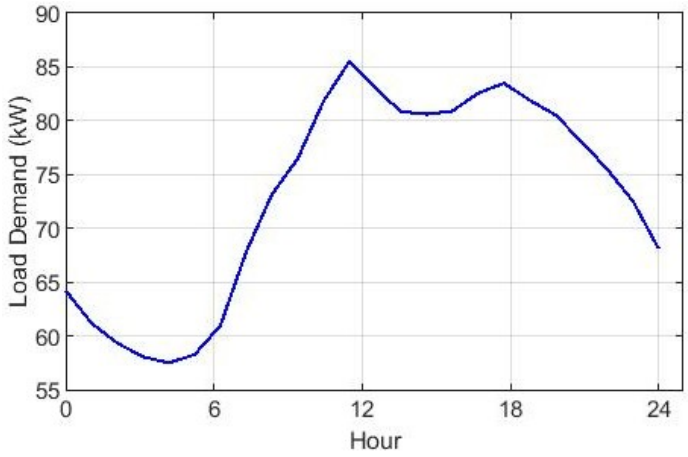

Figure 28 – Average Daily Load Profile of the Community

It is noted that the community has a more important demand in the afternoon than in the morning and does not show a morning and an evening peak. With that in mind, one could consider orienting the panels slightly towards the west to maximize the production in the afternoon when most of the load is concentrated. However, it is also important to note that rotating the panels away from the south will reduce the total energy produced by the PV system. Therefore, let us consider a new irradiance profile where the panels are oriented 20° west of south with an optimal tilt. In PVLIB, the value for orientation is defined as the number of degrees east of north. Therefore, south-facing panels have an orientation of 180° and the new configuration has an orientation of 200° (O200). Yearly, the OS scenario produces 1.05% more energy than the 200° optimal tilt configuration. Both irradiance profiles are compared in Figure 29.

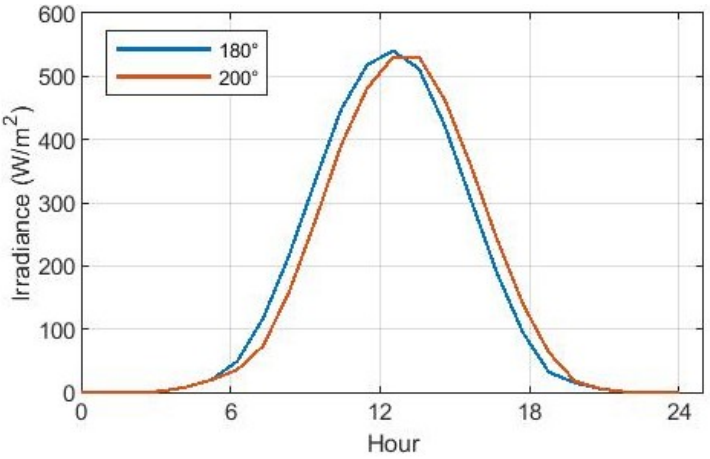

Figure 29 – Average Daily Irradiance Profile for 180° and 200° Orientations

Next, Table 18 compares the simulation results for PV configurations with the OS and O200 irradiance profiles. Also, Figure 30 shows the total monthly production of 100 kW of PV for both irradiance profiles.

Table 18 – Simulation Results for Diesel-PV Configuration Comparing the OS and O200 Configurations

Results	Optimal South	Optimal 200°
Installed PV Capacity (kW)	2.5 - 200	2.5 - 200
Load vs. PV Power Correlation	0.166	0.171
Load vs. PV Monthly Energy Correlation	-0.40	-0.42
PV Penetration (%)	0.5 – 22.0	0.5 – 22.0
PV Curtailment (%)	0 – 50.5	0 – 49.7
Fuel Consumption Reduction (%)	0.5 – 17.7	0.5 – 17.8

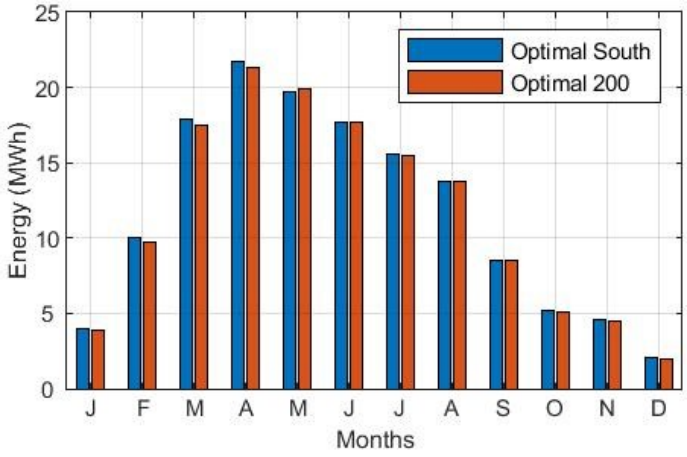

Figure 30 – Total Monthly PV Production – Optimal South vs. Optimal 200° – 100 kW

When compared to the OS scenario, the power correlation for the O200 irradiance profile is improved but the monthly energy correlation is reduced. The simulation results show that the Optimal 200° scenario marginally improves the PV curtailment and penetration as well as fuel reduction for scenarios with high amount of PV installed. For Diesel-PV systems, without WTs, at least 102.5 kW is required to have higher penetration and lower fuel consumption with the Optimal 200° profile than with the OS configuration. For scenarios combining PV with one or up to three

WTs, 92.5 kW of installed PV is required to obtain the same result with OS. However, as mentioned beforehand, those improvements are marginal. Indeed, the maximum improvement in fuel consumption between the OS and Optimal 200° irradiance configurations is a reduction of 0.1% for PV only with 200 kW installed. Therefore, since this proposed solution does not yield substantial gains in fuel savings and a clear reduction in curtailment, it is not considered for the rest of the study. The rest of the analysis will be done considering the OS scenario.

3.5. Analysis

In this subsection, the simulation results are analyzed in terms of their RE penetration, RE curtailment and fuel savings. The OS PV configuration is considered in the analysis since the WS and O200 profiles did not lead to substantial increases in fuel savings. The TT scenario was deemed not worth it because it would require much more maintenance for insubstantial gains in fuel savings. Lastly, the E-W configuration was set aside since there is not enough financial information available to properly compare it to the OS configuration. First, let us consider the RE configurations needed to reach specific amounts of fuel consumption of the diesel power plant. Table 19 lists the different RE configurations which allow the diesel power plant to have a fuel consumption of 170 - 120 kL with 10 kL steps. Initially, without the addition of RE, the diesel consumption was 183.9 kL.

Table 19 – RE Configurations for Specific Fuel Consumption Targets

Installed OS PV (kW)	Number of WTs	Fuel Consumption (kL)	PV Penetration / Curtailment (%)		WT Penetration / Curtailment (%)	
40	-	**170**	9	1	-	-
87.5	-	**160**	16	18	-	-
22.5	1	**150**	5	9	18	4
75	1	**140**	11	31	18	4
47.5	2	**130**	6	43	30	18
130	3	**120**	8	73	36	35

For each reduction of 10 kL of fuel consumption, there is an increase in the required RE generation capacity. For the last four configurations, a significant increase in curtailment for both RE sources is observed.

In general, for the given input data and systems considered, the WT performs better than the PV system in terms of penetration per installed kW and is subject to much less curtailment due to its better correlation with the energy requirements of the microgrid. On the other hand, the PV system does not perform as well. When increasing the PV capacity, the gains in terms of fuel savings tend to diminish as additional production is curtailed, mainly during the summer, when the PV produces most of its energy (Figure 17) and the load demand is at its lowest (Figure 1). However, it is important to note that, in the Canadian Arctic, the capital costs can be almost twice as much for WTs than what they are for PV mainly because of the high transportation costs of WTs [48]. Even though WTs seem to perform better in this setting, designers should consider whether their higher cost can be counterbalanced by the higher associated fuel savings.

Methods considered to reduce the curtailment of the PV system with the objective of increasing fuel savings resulted in slight improvements. However, the curtailment remains high, and the TT

scenario was put aside since it would require more maintenance, which is not deemed worthy of such small gains in fuel savings. Combining PV and WTs allows to increase the penetration of RE and reduce the fuel consumption further than when considering PV or WTs only. However, when increasing the PV installed capacity, the issues of high curtailment and negative correlation with the energy requirements of the grid come up. For example, when computing the PCC comparing the monthly energy requirements of the grid with the energy production of one WT alongside PV, the results range from 0.60, for 2.5 kW of PV, to -0.33 for 200 kW.

Considering the obtained results, one can conclude that the scenarios presented do not seem to be reasonable for medium or high RE penetration because of the high RE curtailment which makes the systems less cost-effective (Table 19). Thus, this study shows the limit of the low penetration regime of RE in a remote Arctic microgrid. Additional elements, such as battery storage, demand-side management, and excess RE recycling through heating would be required to limit the RE curtailment and further increases its penetration and associated fuel savings. Battery storage could allow to reduce RE curtailment while supplying the RE production to the microgrid when required. Demand-side management, more precisely demand response, could improve the correlation and matching between the RE supplied and the load of the community.

Optimization is out of the scope of this research work. However, it would be required to identify the optimal configuration of PV and WTs for this specific setting. Some of the parameters that should be considered are: 1) the capital costs of the wind and PV systems, 2) the O&M costs of the power plant, 3) the cost of diesel and 4) the GHG emissions.

Established approaches to optimize the sizing of PV and WTs already exist. A common method is the creation of a parametric objective function based on parameters similar to the ones aforementioned and the use of an optimization method to identify the best scenario [49], [50], [51].

Lastly, since PV and WTs are intermittent sources of energy, it would be relevant to repeat the current study with solar and wind datasets from different Arctic communities to confirm whether these findings can be generalized.

Chapter 4 - Electrification of Space Heating

In the remote Arctic community considered in the study, the electric demand, which was used for the first part of the study, represents only 27% of the total energy use. On the other hand, heating needs correspond to 37% of the total energy used [9]. The remaining 35% of energy use is for local transport in the community. Since most Canadian Arctic communities use oil for their heating needs [20], this load should also be considered when trying to reduce GHG emissions. Up until now, the study only considered the energy required by appliances and lighting, which are the only electrified loads in the Arctic remote community considered in the study.

In this section, additional space heaters, which allow to electrify a portion of the heating demand of the community are considered along with the Diesel-PV-Wind power plant. The heaters considered are Electric Thermal Storage (ETS) units, which allow to store heat in dense bricks, for a long period of time, and circulate it when required. The objective of this scenario is to recycle the excess RE generation through space heating thus reducing the heating oil consumption.

4.1. Small Arctic Community Space Heating Load Modelling

In remote Arctic communities which utilize oil as a heating source, furnaces are fired locally in all buildings to provide heat. Since the production of heating energy is not centralized as it is for the electricity generation power plant considered in this study, it is hard to have access to data related to the heating load profile of a community. Therefore, the space heating load of the community was estimated based on the buildings' characteristics.

First, information regarding the population, the number of occupied houses and the identification and state of specific buildings was obtained from the community. All buildings were labelled, categorized by type, and had their footprint measured using Google Earth (Figure 31). Also, Table 20 presents examples of buildings that were identified and measured to model the space heating requirements of the community.

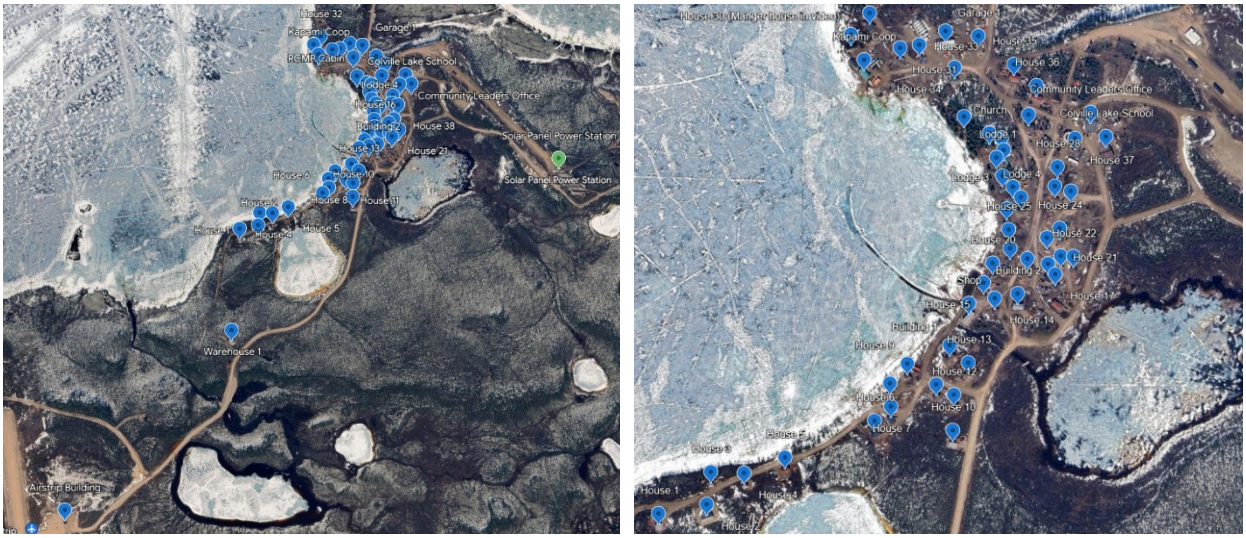

Figure 31 – Map of the Considered Community

Table 20 – Example of Buildings Identified and Measured

Building Name	Building Type	Floor Area (m^2)
Garage 1	Warehouse	185
RCMP Cabin	Small Offices	56
Health Station	Hospital	254
School	School	359
Lodge 1	Small Hotel	195
House 1	house	126

A total of 40 houses were identified and modelled. On the other hand, the hospital and school buildings are unique while there are two retail buildings, four small hotel buildings, five small offices and lastly five warehouses. Then, specific EnergyPlus Input Data Files (.IDF) building models, considering Arctic conditions, were obtained from the US Office of Energy Efficiency & Renewable Energy to represent the community [52]. These prototype building models represent the characteristics of commercial and residential buildings across numerous climate zones in the US, such as wall insulation, number and type of windows, heating equipment and typical yearly load schedules. In this study, residential, health, school, hotel, office and warehouse prototypes for Fairbanks, Alaska are used. Also, the prototype buildings were selected with an old construction date since information from the community stated that a large majority of buildings required major repairs.

The following methodology was used to obtain the heating load dataset. Using an EnergyPlus Weather (.EPW) file of the considered community, which was obtained from the Canadian Weather Year for Energy Calculation (CWEC) [21], simulations were run in the EP-Launch app for each .IDF building model considered. Using the IDF Editor in the app, meters were created to output the yearly hourly-level space heating load profile of each prototype building at the end of the simulation. Lastly, for every building type, the load profiles are adjusted based on the measured building area mentioned earlier and the footprint of the EnergyPlus building model. A similar approach was proposed in [53]. However, it did not consider EnergyPlus simulations to obtain hourly values. Furthermore, the annual energy required to heat the buildings of the community was obtained [9]. That value was divided into two portions, one for the residential buildings and the other for the rest of the buildings. Since this total heating value represents both space and water heating, it was adjusted to represent only the portion associated with space heating. For residential buildings located in Canadian Northern territories, space heating represents 76% of the total heating requirements [54]. Therefore, this allowed to normalize the space heating profiles obtained in the EneryPlus simulation to reflect the measured data. The aggregated profile, for all buildings combined, is presented in Figure 32. This corresponds to the total end use power required to heat the buildings of the community, before considering the efficiency of the heaters. The space heating demand of the community varies a lot over the year. It reaches a high during the winter months and a low during the summer months similarly to the electrical demand of the community, shown in Figure 1. However, in the case of the heating load, the difference of load between the colder and warmer months is more significant.

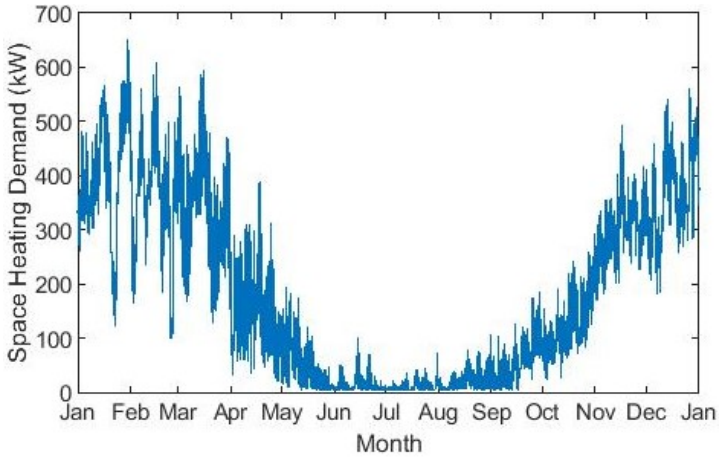

Figure 32 – Aggregated Space Heating Yearly Load Profile

To evaluate the oil consumption for space heating as well as the potential to recycle excess RE generation through heating, the efficiency of different heating devices considered in the study are presented in Table 21 [55], [56].

Table 21 – Efficiencies of Considered Heating Devices

System	Efficiency (%)
Oil Furnace	80
Electric Heater	100

Furthermore, determining the electric distribution efficiency of the microgrid is required to calculate the electric power required at the power plant to charge the ETS units in the buildings. Since there is no detailed information available regarding the distribution system of the community considered in the study, a distribution efficiency of 90% was established after discussing with colleagues from CanmetENERGY-Varennes who have modelled the microgrid of a similar small Arctic community for which much more information was available [3].

Then, based on those efficiencies and the heating datasets presented above, a simulation is run to calculate the total amount of energy required and heating oil consumed for space heating. The total end use heating requirement of the community is 1941 MWh. In this study, a conversion rate of 10.67 kWh/L is used for heating oil [9].

Table 22 presents the distribution of the end use energy demand by building type.

Table 22 – Portion of Total Energy for Different Energy Sectors

Building Type	Total Heating Oil Consumption without ETS (kL)
Residential	83.1
Health Centre	11.4
School	10.8
Small Hotel	6.9
Small Office	19.6
Warehouse	50.2
Total	**182.0**

4.2. Electric Thermal Storage (ETS) Modelling

To evaluate the potential to recycle excess RE generation through heating and further reduce curtailment and GHG emissions, a new configuration of the power system is considered. An updated power system model, containing spacing heating, is shown in Figure 33.

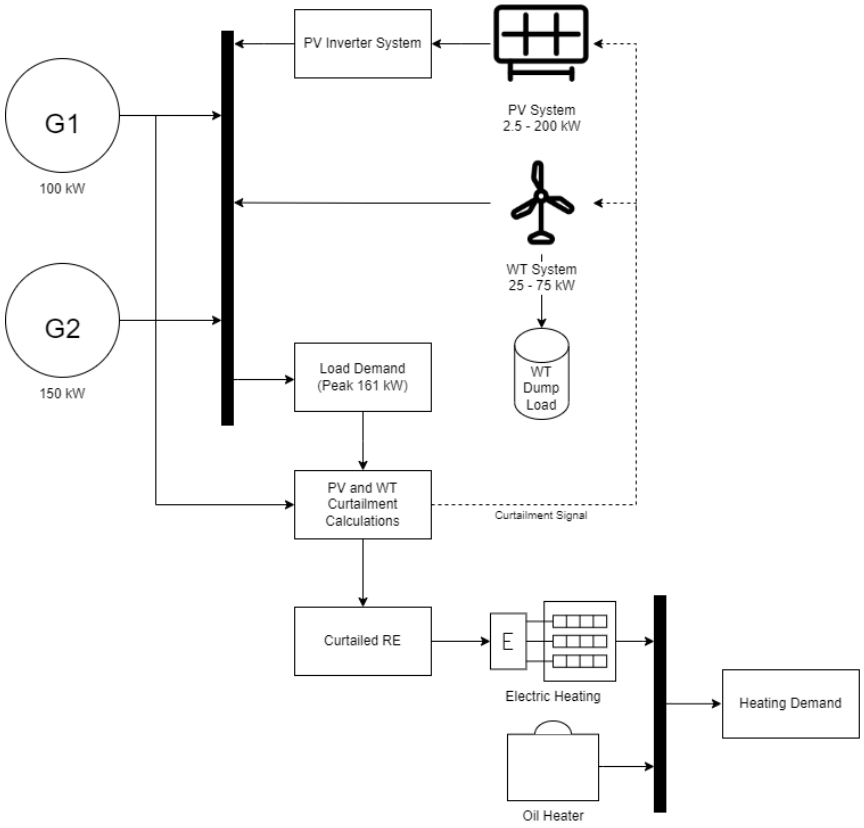

Figure 33 – Diagram of Modelled Power System With Heating

As in Figure 4, the diagram contains two diesel generators, paired with both PV and WT systems. In this configuration, the microgrid controller also matches the power generation to the load demand, considering the DGS's minimum loading requirements. However, when curtailment is required, the excess RE is sent to the ETS units to charge them, so it can be recycled through space heating. If the units can no longer be charged, the RE systems will be curtailed as in the first study.

The model used in section 2.4 is modified to redirect some of the excess RE generation, which would have been curtailed in the earlier scenario, to electric thermal storage (ETS) systems. These devices, which are mainly produced by Steffes [16], a manufacturer from North Dakota, USA, use electric elements to store heat in high-density bricks, which are well insulated and can hold energy for long periods of time. When required, a fan blows air through the bricks to circulate heat by convection. Although it is usually used for peak shaving, ETS coupled with a smart grid can increase a system's variable RE capacity and ultimately reduce curtailment [11], [14]. It is also interesting to note that ETS is much cheaper than electrochemical battery storage. In this current study, ETS units will be considered as an auxiliary source of heat, along with the already existing

oil furnaces. Using these devices in a remote northern microgrid along with RE has the potential to stabilize the network by creating a better balance between the production and the demand by supplying excess RE generation to the ETS heaters which would otherwise be wasted [19].

The thermal energy stored in the ETS is defined as

$$E_{ETS} = C(T_{ETS} - T_{Ambient}) \tag{6}$$

where C is the thermal capacity of the system. The value used in the model was provided by Steffes [57]. T_{ETS} is the ETS core temperature (°C) and $T_{Ambient}$ is the house temperature (°C), considered as a constant 20 °C in the current study.

To model the ETS system, the following logic is considered: at every time step, the ETS system's energy storage ($E_{ETS}(t)$) varies as shown in (7). It can be charged electrically with excess RE generation ($P_{ETS}^{in}(t)$). The excess RE production is converted to heat by the resistive elements of the ETS. Also, it is equipped with a fan to circulate heat into the room ($P_{ETS}^{heat}(t)$), and it has small standby losses ($P_{ETS}^{loss}(t)$). Operating the fan to circulate heat requires a small amount of power, which is neglected for this current study.

$$E_{ETS}(t+1) = E_{ETS}(t) + (P_{ETS}^{in}(t) - P_{ETS}^{heat}(t) - P_{ETS}^{loss}(t))\Delta t \tag{7}$$

Through a literature review related to ETS modelling [11], [12], [13], [14], [15], some interesting elements are identified to improve the accuracy of the model. Most importantly, it is noted that both the maximum output power and the standby losses of the ETS depend on the device's current state of charge (SoC), which is directly related to the core temperature of the device, T_{ETS}. Unfortunately, ETS manufacturers do not provide documentation, such as discharge curves depending on the stove's SoC, to accurately represent these phenomena. For that reason, some of the considered studies do not set a limit on the available output power. As for the standby losses, some of the studies set an arbitrary value while others neglect them. However, in [15], Moffet et al. present the model of a central ETS system based on experimental data obtained from Hydro-Québec Research Institute (IREQ). The paper proposes empirical equations to represent the maximum available heating power output of the ETS, as well as its standby losses, based on the average core temperature of the device at a given moment. Conclusions from the literature show that modelling the losses and available output power of the ETS from a single-point averaged core temperature is appropriate [12], [18].

The device modelled in [15] is the Steffes DLF30B, a central residential ETS unit that is no longer commercially available. In more recent publications [17], [58], researchers from Hydro-Quebec published curves representing the behaviour of another ETS unit, the Steffes 2103, which has a rated charging input of 5.4 kW ($P_{ETS\,Max}^{in}$) and a storage capacity of 20.25 kWh [59]. Using the same logic proposed in [15], equations were obtained from the Steffes 2103 performance curves to represent the standby losses (P_{ETS}^{loss}) and the maximum output heating power available ($P_{ETS\,Max}^{heat}$) based on the core temperature (T_{ETS}) of the device. These relations are defined in equations 8 and

9. When the input power exceeds the output power, the core temperature of the ETS increases thus charging the unit. Otherwise, the unit is discharging, which reduces its core temperature. Both the input and output power are controllable. The first is controlled by energizing one, or many, of the unit's heating elements when there is excess RE production available and the latter by adjusting the fan speed.

$$P_{ETS\,Max}^{heat} = 1.44 \cdot 10^{-8} T_{ETS}^{3} - 2.37 \cdot 10^{-5} T_{ETS}^{2} + 1.46 \cdot 10^{-2} T_{ETS} + 0.23 \quad (8)$$

$$P_{ETS}^{loss} = 9.41 \cdot 10^{-4} T_{ETS} - 0.06 \quad (9)$$

To maximize oil savings and minimize RE power curtailment, the ETS heaters considered in this study are charged with as much available excess RE ($P_{Available}^{in}$) possible until the ETS reaches its maximum SoC. Steffes 2103 units are equipped with four heating elements. Therefore, its charging input can vary by power increments (P_{inc}) of 1.35 kW. Mathematically, the number of elements activated is obtained by calculating the floor ($\lfloor \rfloor$) of the Excess RE available ($P_{Available}^{in}$) divided by the power increment (P_{inc}) of the unit. The charging input is limited at $P_{ETS\,Max}^{in}$ when the available charging power ($P_{Available}^{in}$) exceeds 5.4 kW. Also, if the ETS heater reaches its $SoC_{ETS\,Max}$, charging is not allowed. This logic is detailed in equations 10 and 11.

$$SoC_{ETS} < SoC_{ETS\,Max} \Rightarrow P_{ETS}^{in} = \begin{cases} P_{ETS\,Max}^{in} & P_{Available}^{in} \geq P_{ETS\,Max}^{in} \\ \left\lfloor \frac{P_{Available}^{in}}{P_{inc}} \right\rfloor P_{inc} & P_{Available}^{in} < P_{ETS\,Max}^{in} \end{cases} \quad (10)$$

$$SoC_{ETS} = SoC_{ETS\,Max} \Rightarrow P_{ETS}^{in} = 0 \quad (11)$$

Next, $P_{ETS\,Max}^{heat}$ represents the available output power at a given time based on the core temperature of the system. P_{ETS}^{heat} is the actual heat power circulated into the room, which can range from zero to $P_{ETS\,Max}^{heat}$ depending on the speed of the fan. Since the power consumption of the fan is not considered in the study and the manufacturer does not provide information regarding the relation between the fan speed and the ETS output power, this component will not be specifically modelled. It is simply supposed that the fan speed varies so that P_{ETS}^{heat} corresponds to the dispatched ETS power detailed in equations 12 and 13. For the Steffes 2103 room unit, the fan power consumption represents 0.5 – 2% of the rated input power of the device [59]. Furthermore, in his masters' thesis exploring the potential of ETS to help the decarbonization of commercial buildings, Chabot states that the consumption of the motor that powers the fan is negligible when evaluating the efficiency of ETS systems [12]. On the other hand, P_{ETS}^{loss} represents the standby losses of the system and cannot be controlled. Also, since the losses leak from the core of the ETS into the building, they are considered as part of the total heat supplied by the ETS heater (P_{Elec}^{heat}). The same assumption is made in other studies [12], [15]. These state that it is reasonable to include the ETS losses (P_{ETS}^{loss}) as part of the power provided by the ETS (P_{Elec}^{heat}) because the heat that leaks out of the heater will distribute itself around the house and contribute to the heating requirements.

$$P_{Elec}^{heat} = P_{ETS}^{heat} + P_{ETS}^{loss} \tag{12}$$

$$P_{Elec\ Max}^{heat} = P_{ETS\ Max}^{heat} + P_{ETS}^{loss} \tag{13}$$

Then, P_{ETS}^{heat} is prioritized over P_{Oil}^{heat} to reduce the heating oil consumption and the associated GHG emissions. When controlling P_{ETS}^{heat}, two different scenarios can arise. First, as defined in equation 14, if the total available power from the ETS ($P_{Elec\ Max}^{heat}$) is higher than the heating demand (P_{Demand}^{heat}), the ETS solely meets the thermal power to maintain the temperature at the reference point. The heat demand is met by adjusting the fan speed to control the output ETS power, (P_{ETS}^{heat}) while the standby losses (P_{ETS}^{loss}) are not controllable. Thus,

$$P_{Elec\ Max}^{heat} \geq P_{Demand}^{heat} \Rightarrow P_{Oil}^{heat} = 0,\ P_{ETS}^{heat} = P_{Demand}^{heat} - P_{ETS}^{loss} \tag{14}$$

On the other hand, if the heating demand cannot be met by operating the ETS heater at its maximum power available ($P_{ETS\ Max}^{heat}$), the oil furnace will complement the ETS unit to provide the heat required.

$$P_{Elec\ Max}^{heat} < P_{Demand}^{heat} \Rightarrow \begin{matrix} P_{Elec}^{heat} = P_{Elec\ Max}^{heat}, \\ P_{Oil}^{heat} = P_{Demand}^{heat} - P_{Elec\ Max}^{heat} \end{matrix} \tag{15}$$

In a real-life scenario, this could be done with a smart thermostat and a controller, which first turns on the ETS to maintain the room temperature at the desired setpoint. If the ETS heater is heating at its max available power and the room temperature setpoint is still not met, the oil furnace would supply the remaining heating requirements. Alternatively, setting the ETS units to a higher setpoint than the one used for the oil furnace would also prioritize the ETS unit. Lastly, equation 16 defines how the heating needs of the buildings are met and Figure 34 presents a diagram of the space heating model.

$$P_{Demand}^{heat} = P_{ETS}^{heat} + P_{ETS}^{loss} + P_{Oil}^{heat} = P_{Elec}^{heat} + P_{Oil}^{heat} \tag{16}$$

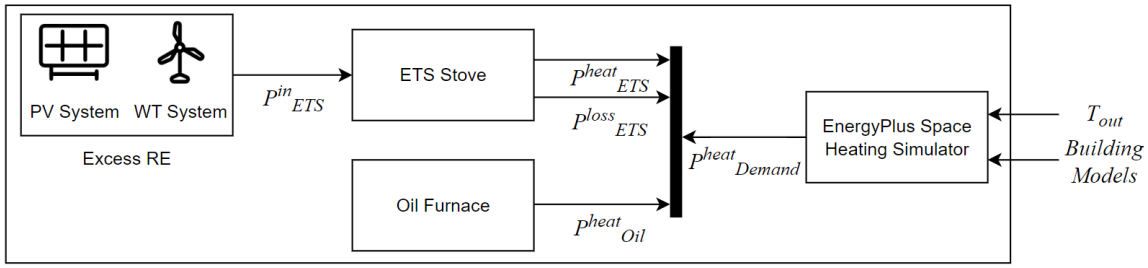

Figure 34 – Diagram of Space Heating Modelling

Then, Steffes ETS systems are equipped with brick core and outdoor temperature sensors, T_{out}, which allow the system to control its maximum core temperature and associated SoC based on the outdoor temperature. In the equipment documentation, different strategies are proposed for the

brick core charge control [60]. In this study, the Automatic Charge Control is considered. For that mode, a Start Brick Core Charge and a Full Brick Core Charge outdoor temperature setpoints are defined. For the 2100 series, these values are 16 °C and -7 °C. These values are deemed acceptable for the current study after observing Figure 35, which compares the daily average outdoor temperature to the daily residential heating requirements.

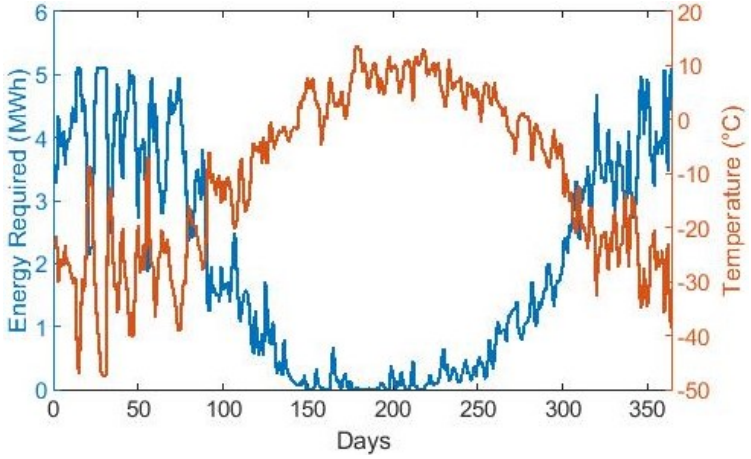

Figure 35 – Daily Residential Heating Requirements vs. Average Outdoor Temperature

Next, the documentation states that the 2100 series units can set the core charge setpoint to a maximum of 593 °C and a minimum of 93 °C. Therefore, the algorithm developed to represent the charge control of the ETS, which corresponds to the maximum allowed core temperature, is defined in equation 17:

$$T_{ETS\ Max} = \begin{cases} 593 & T_{out} \leq -7 \\ -21.7T_{out} + 440.8 & -7 < T_{out} < 16 \\ \text{ETS turned off} & T_{out} \geq 16 \end{cases} \quad (17)$$

When applying equation 17 to the outdoor temperature dataset used in this study, the profile of the maximum SoC allowed over time is obtained. A SoC of 1 corresponds to the energy stored in the bricks when the core temperature reaches 593°, as per (6). It is shown in Figure 36.

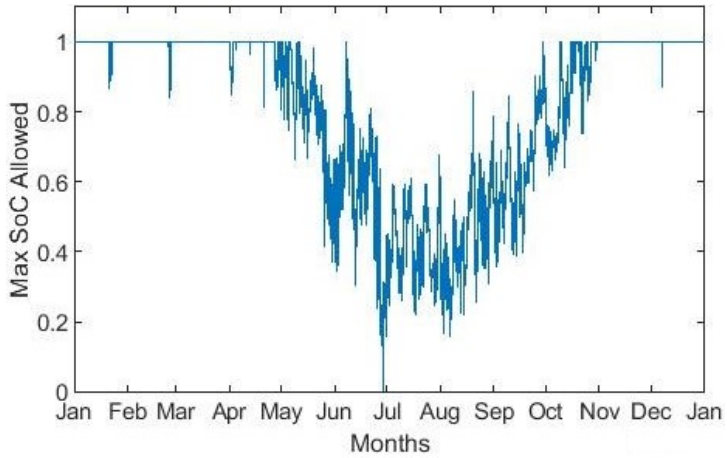

Figure 36 – Maximum Allowed SoC Based on the Charge Control Algorithm

Lastly, based on the maximum allowed core temperature of the ETS, the charging input of the heater (P_{ETS}^{in}) is limited to zero if the measured core temperature reaches its maximum allowed value, as per (17), and is allowed again when the temperature drops below that same value. However, a tolerance band of ± 5 °C (or just under 1% for the SoC) is added to the model to avoid continuously turning on or off the heating elements. For example, if $T_{ETS\ Max}$ is set to 500 °C, the heating elements will be turned off is the temperature reaches 505 °C and turned on if the temperature drops down to 495 °C. Also, the amount of heating elements activated to charge the ETS is determined, as previously mentioned, to minimize RE power curtailment.

The maximum SoC associated to the maximum allowed core temperature corresponds to $SoC_{ETS\ Max}$ in equations 8 and 9. Lastly, in the model, it is supposed that the Automatic Charge Control calculates the average outdoor temperature hourly and sets the according $T_{ETS\ Max}$ for the next hour.

To conclude, the ETS model and its associated equations were validated in partnership with Hydro-Québec based on publications [19], [58] and associated experimental data.

4.3. ETS MATLAB Simulink Model

This section presents the ETS MATLAB Simulink model (Figure 37) that is based on the equations defined in section 4.2.

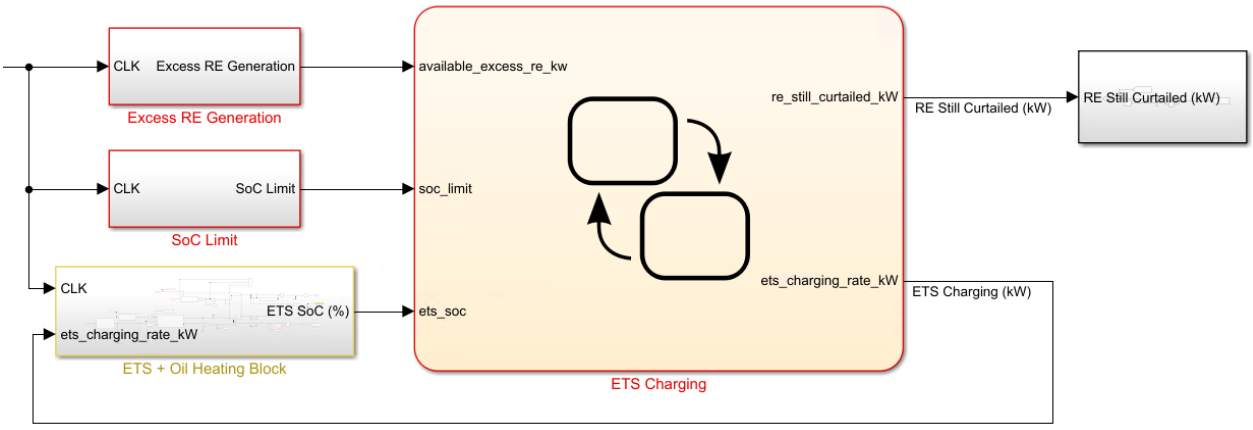

Figure 37 – MATLAB Simulink ETS Model

The ETS model is based on a Simulink Stateflow block (ETS Charging) which sets the charging rate of the ETS system based on the available excess RE, the maximum core temperature allowed ($T_{ETS\ Max}$) and the current core temperature of the ETS (T_{ETS}). In the model, the temperature values are converted to SoC, using equation 6. It is based on the equations 10 and 11 defined in section 4.2. If the ETS is full, based on the inputs soc_limit (equation 17) and ets_soc, charging will be stopped. When the ETS is allowed to charge, the charging rating (ets_charging_rate_kW) is set by the Stateflow block depending on the availability of excess RE (available_excess_re_kW) and limited by the maximum charging rating of the ETS. The ETS Charging block also outputs the amount of excess RE that remains curtailed, re_still_curtailed_kW.

Then, the ETS + Oil Heating block of the model includes the remaining equations that were defined in section 4.2. This block takes care of the relationship between the inputs and outputs of the ETS and adjusts its SoC accordingly. It is also responsible for managing the heat circulated from the ETS to the room, based on the device's SoC and the heating requirements. For every time step, it does the following operations:

1) Based on the current T_{ETS}, P_{ETS}^{loss} and $P_{ETS\,Max}^{heat}$ are calculated. (equations 8 and 9)

2) Based on P_{Demand}^{heat}, P_{ETS}^{loss} and $P_{ETS\,Max}^{heat}$, P_{ETS}^{heat} and P_{Oil}^{heat} are calculated. (equations 12 to 16)

3) Based on the inputs and the outputs of the ETS unit, T_{ETS} and the SoC can be calculated for the next timestamp. (equations 6 and 7)

4.4. Correlation Analysis Between Heating Load and RE Generation

To assess the potential for ETS to recycle excess RE production through space heating, the match between these two metrics needs to be evaluated. In the literature, some studies have considered RE generation for space heating needs in northern climates. In [61], Bolt et al., researchers from the University of Alaska Fairbanks and Stanford University, propose a simple method to analyze the match between heating requirements and excess RE production. They first suggest that, in colder regions, building heat loads are positively correlated with wind energy production and negatively correlated with PV energy. Therefore, they conclude that wind is a better fit for space heating than PV. Lastly, it is mentioned that there is a lack of specific studies in the literature that integrate heating loads with RE in remote Arctic microgrids. Beyer et al. [62] also propose that wind energy is a good match for space heating in colder climates. First, the study shows that wind speeds generally peak during the winter and that an increase in wind speed leads to more heat losses and infiltration in buildings, which increases the space heating requirements. These phenomena lead to an improved correlation between wind speed and space heating requirements. With all that information in mind and given the fact that ETS provides an added storage element to the power system, the maximum number of WTs considered in the simulation scenarios will go up from three to five for this section. Furthermore, ETS systems have been proven to be effective to recycle excess RE generation through heating in Arctic conditions. For example, in the microgrid of Kongiganak, a remote community of around 500 in Alaska, twenty-one residential ETS devices, rated at 6 kW for charging with 31 kWh of thermal storage, were installed to recycle excess RE production from the five installed 95 kW WTs. The WTs were sized specifically, close to 200% of the peak electric load, to produce enough energy for both the base electric load of the community and to charge the ETS stoves. On average, the households equipped with ETS systems reduced their heating oil consumption by 50% [10]. For the current study, since the ETS system modelled is a residential unit and that the houses of the community account for almost half of the total heating requirements, the addition of ETS units will only be considered in these buildings.

First, the PCC is used to evaluate the match between the RE production, before curtailment, and the residential space heating requirements, similarly to what was first done in the Renewable Energy Low Penetration Utilization Analysis Chapter. Table 23 presents the correlation between

the heating load and both the total PV and WT production, without considering curtailment. The results are in agreement with the findings in the literature.

Table 23 – Correlation Results Between Heating Requirements and Produced RE

Correlation / Scenarios	Power	Monthly Energy
Heating Load vs. PV Production	-0.208	-0.570
Heating Load vs. WT Production	0.077	**0.530**

In terms of instantaneous power correlation, there is no notable link between the heating load and the WT production. As for between the heating load and the PV production, there is a weak negative correlation. The results are similar to what was observed when evaluating the correlation between the RE production and the electrical load demand and more specifically when focusing on the monthly energy correlation. Indeed, there is a significant negative correlation between the PV production and the heating requirements. As for between the WT production and the space heating, the correlation is positive. Therefore, this would suggest that WTs are better suited than PV panels to supply the space heating load of the community.

Figure 38 presents the monthly excess RE for two scenarios and compares them to the monthly residential space heating requirements.

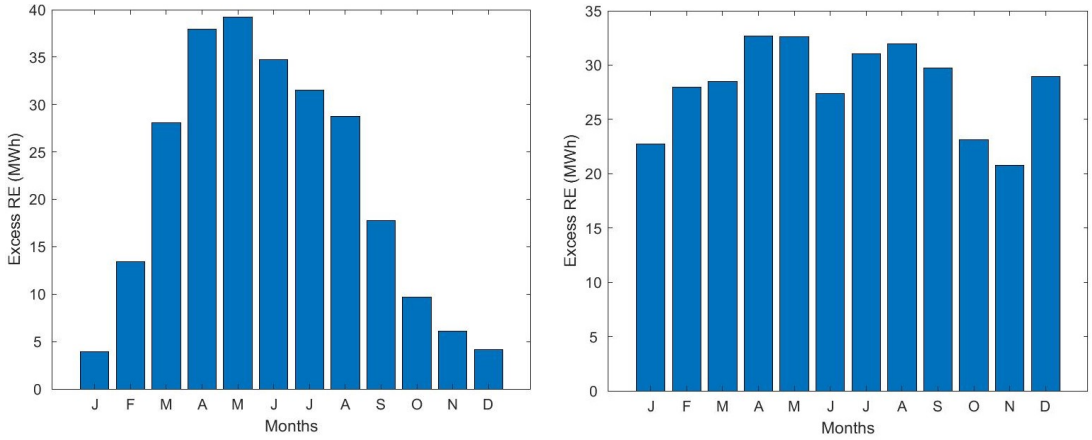

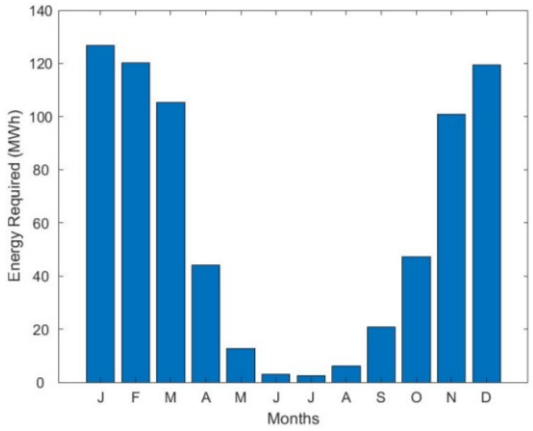

c)

Figure 38 – Comparison of Monthly Energy – a) Excess RE for 2 WTs and 200 kW PV, b) Excess RE for 5 WTs and 5 kW PV and c) Residential Space Heating Requirements

These results tend to indicate that, with more installed WTs, there will be more power available to charge the ETS systems during the winter months during which the heating demand is at its highest.

Next, since the ETS system includes storage, it can be interesting to evaluate the delayed similarity between the residential heating requirements and the excess RE generation. The cross-correlation coefficient measures the similarity between two data sequences for different time shifts. In this study, it is used to compute the correlation between the time shifted RE production and the space heating load demand. When the cross-correlation reaches a maximum for a time shift different than zero, it can show that energy storage could be beneficial to improve the match between the excess RE and the power requirement, which corresponds to the heating needs in this case [63].

Before calculating the cross-correlation coefficient, the daily average profile for residential space heating (Figure 39) and excess RE generation for various configurations (Figure 40) are presented. In those figures, each time step, for example 6:00, represents the average value for that same time step throughout the year.

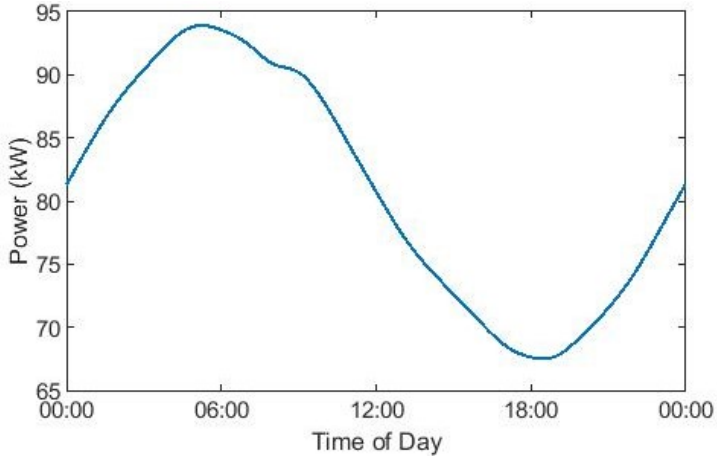

Figure 39 – Daily Average Residential Space Heating Requirements

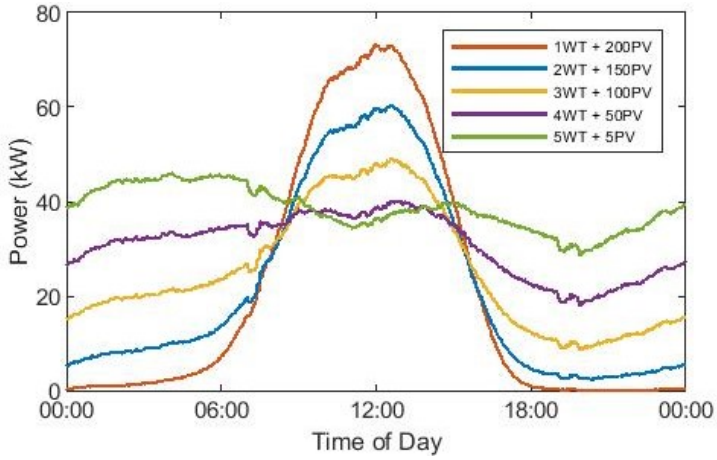

Figure 40 – Daily Average Excess RE Profile for various RE Configurations

The heating requirements of residential buildings tend to peak from 0:00 to 12:00. As for the excess RE daily profiles, adding more PV shifts the peak to the middle of the day, when the sun is at its highest. On the other hand, when the RE configuration is more concentrated on WTs, the daily profile is much more constant, with a small peak in the early hours of the day. Then, the cross-correlation between the hourly excess RE generation and the hourly residential space heating requirements is calculated considering the same RE configurations as shown in Figure 40 as well as for configurations with PV or WTs only. These results are presented in Figure 41. The y-axis corresponds to the correlation value while the x-axis corresponds to the time shift between the excess RE production and the heating requirements.

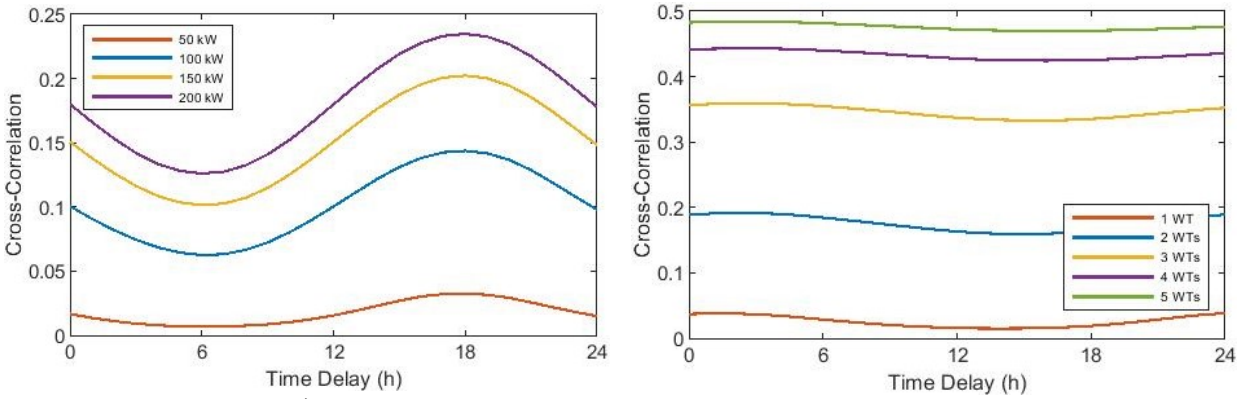

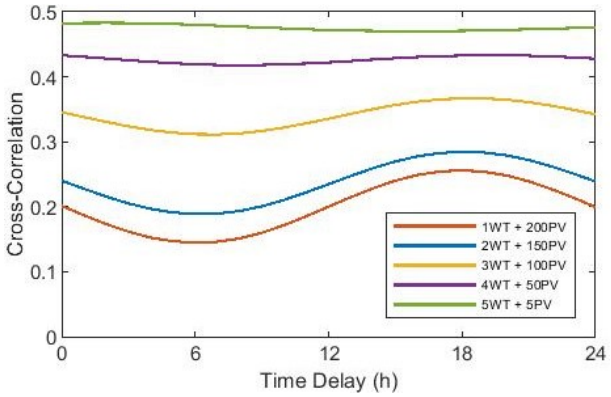

c)

Figure 41 – Cross-Correlation Between Excess RE Configurations and Residential Heating Requirements – a) PV only, b) WTs only and c) PV + WTs

From that figure, one directly notices that the overall match, or correlation value, between the excess RE and the heating requirements is higher with WTs than it is with PV. For configurations with PV only (a), the cross-correlation increases for all time delays when adding more panels and it peaks at a delay of 18h for all PV ratings, which corresponds to the delay between the solar peak production around noon (Figure 41) and the peak heating demand around 6 AM (Figure 39). Even though the correlation coefficient between two datasets is not affected by the magnitude of the values, the installed PV capacity has an effect on the correlation because it modifies the profile of the excess RE generation, as seen in Figure 40. As for RE configurations with WTs only, the cross-correlation is higher than it was for PV, and it also increases when adding more installed capacity. The cross-correlation peaks at a time delay of around 2 to 3h since the peak wind production occurs around 3 AM (Figure 40). When combining PV and WTs (c), with at least 50 kW of PV, the cross-correlation peaks with a delay of 18h between the excess RE and the space heating requirements. For the last curve, with 5 WTs and 5 kW PV, the cross-correlation peaks with a 2h delay. Since the cross-correlation peaks at non-zero values for all configurations and that the RE production can be unpredictable, one can conclude that the storage element offers an added value to further reduce fuel consumption. Lastly, for RE configurations with a lot of PV, the energy will remain stored in the ETS system for longer periods of time before it is circulated to the building and could lead to higher standby losses. Indeed, a simulation was run considering a full ETS unit as an initial condition with no power input or output. This allowed to identify the effect of ETS losses over time and how the SoC decreases. These results are detailed in

Table 24.

Table 24 – Effect of ETS Losses on SoC Over Time

ΔT (h)	SoC
0	1
6	0.84
12	0.71
18	0.61
24	0.52

30	0.44
36	0.38
42	0.33
48	0.29

4.5. ETS Model Simulation Results and Analysis

After having modelled the ETS system, the next objective is to evaluate its potential to reduce the consumption of heating oil in remote communities. First, simulations based on the modelled heating load profiles are run to calculate the amount of heating oil consumed in the residential buildings of the community. In this scenario, the oil furnaces supply the entirety of the heating demand. For the 40 houses considered in this study, the yearly oil consumption is 83.1kL or 2.08 kL per home.

Then, the ETS heaters are introduced in the simulations. The first scenario evaluates the potential to recycle excess RE generation and reduce heating oil consumption for different configurations of installed RE and ranging numbers of residences equipped with a single Steffes 2103 unit. More specifically, the PV capacity ranges from 5 to 200 kW with an OS configuration, the number of installed WTs varies from 1 to 5 and the number of houses equipped with a Steffes 2103 ranges from 10 to 40, with increments of 10. For ETS integration scenarios, the installed PV capacities used in the simulation results are 5, 50, 100, 150 and 200 kW to reduce the number of simulations and limit the total simulation time.

First, let us dive into specific configurations to further understand the behaviour of ETS heaters and analyze the obtained results. First, Figure 42 shows detailed simulation results for a scenario where 10 houses are equipped with an ETS unit alongside a RE configuration of 1 WT and 50 kW of PV. For this scenario, 54% of the excess RE generation is recycled and the heating oil fuel consumption of the 10 houses is only reduced by less than 4%. Figure 42-a) and c) represent the aggregated charging power and heating power for all 10 houses.

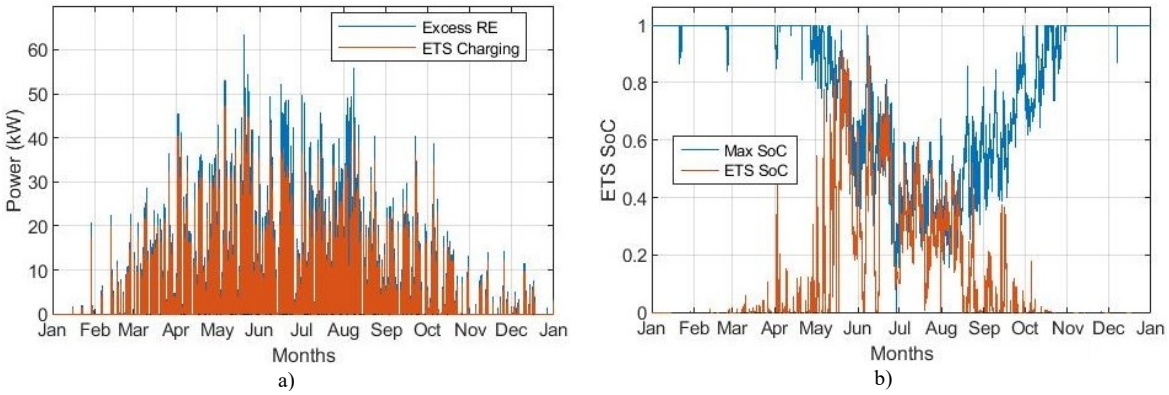

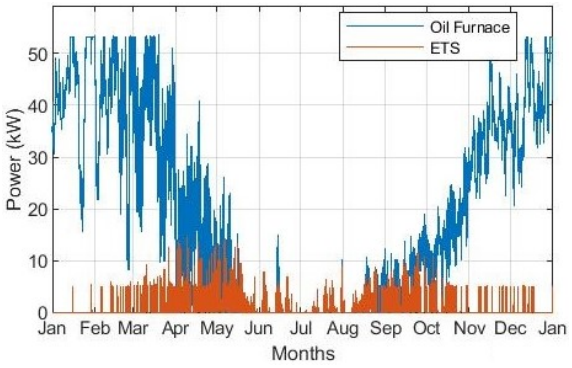

c)

Figure 42 – ETS Simulation Results - 10 ETS 1 WT + 50 kW PV: a) Excess RE and ETS Charging, b) ETS SoC and c) Oil Furnace vs. ETS Output

Here, one can quickly conclude that the installed RE is insufficient to be paired with ETS units to make a significant impact in the reduction of heating oil consumption. Indeed, with that configuration, the curtailment is not high enough to provide substantial excess production and charge the ETS system, mostly during the winter months (a). Therefore, the ETS SoC (b) cannot reach its reference value outside of the May to August period. This leads to little contribution of the ETS during the winter, when there is no RE excess available, and during the summer, when the space heating requirements are low (c).

Next, Figure 43 presents the results for the configuration with 10 ETS heaters, 5 WTs and 150 kW of PV. For this scenario, only 26% of the excess RE is recycled while the fuel savings reach 13 kL, or 63% per home.

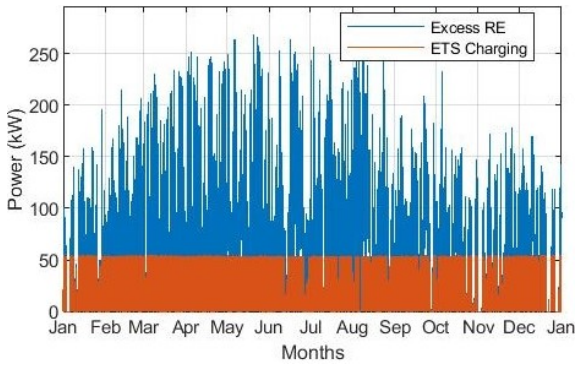

a)

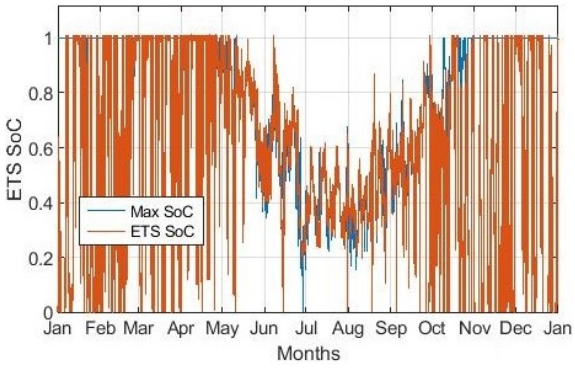

b)

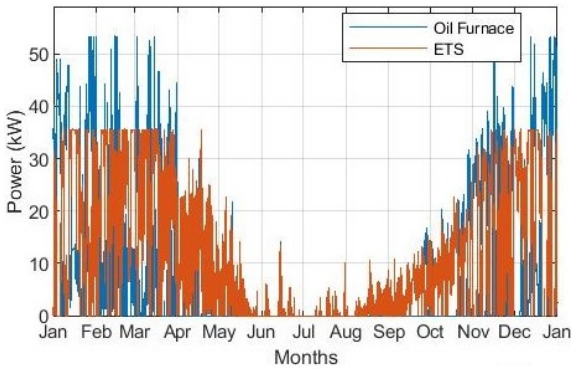

c)

Figure 43 – ETS Simulation Results - 10 ETS 5 WTs + 150 kW PV: a) Excess RE and ETS Charging, b) ETS SoC and c) Oil Furnace vs. ETS Output

In this case, the excess RE production is plentiful and allows the ETS to be charged close to its maximum storage capacity for most of the year, unless when the maximum SoC allowed is reduced, as shown in Figure 36, when the outdoor temperature is higher and the heating requirements are therefore reduced. Indeed, as we can see on Figure 43-b), the SoC is reduced during the warmer months of the year, even if there is plenty of available excess RE and the ETS output is low. This prevents the ETS units from storing high amounts of energy when the heating requirements are low. If the heaters were allowed to maintain their core temperature much higher, it would lead to unnecessary thermal losses in the ETS which would overheat the house when the outside temperature is warm. For this scenario, one could also conclude that the RE configuration is oversized to supply only 10 ETS units. Indeed, the excess RE is almost always at least twice as high as 54 kW, the rated power of 10 Steffes 2103 units. To further support that argument, supplying 10 ETS units with one less WT provides almost the same heating oil savings, 58% instead of 63%.

Lastly, Figure 44 shows the simulation results for a scenario with 20 ETS units, 5 WTs and 50 kW PV. With that configuration, 52% of the excess RE is recycled and the heating oil savings reach 20 kL, or 48% per home.

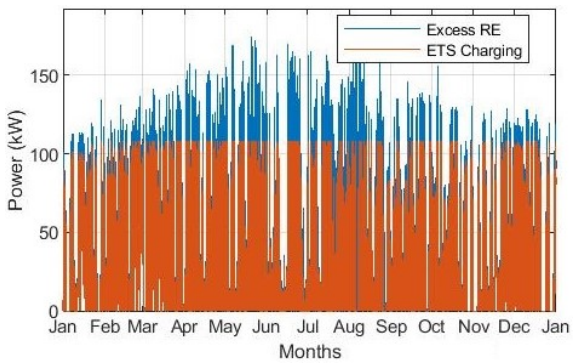

a)

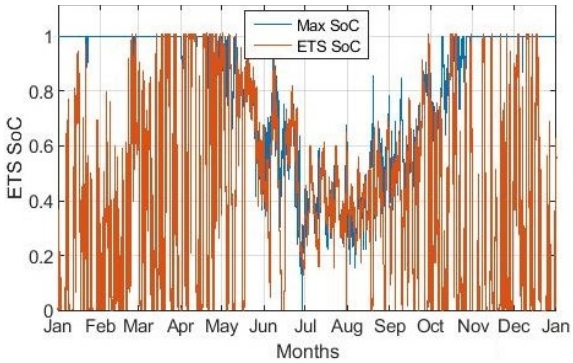

b)

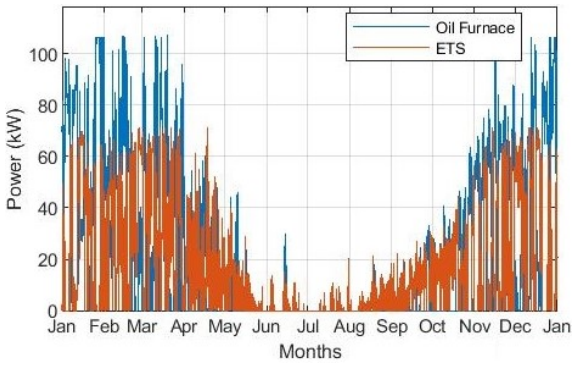

c)

Figure 44 – ETS Simulation Results - 20 ETS 5 WTs + 50 kW PV: a) Excess RE and ETS Charging, b) ETS SoC and c) Oil Furnace vs. ETS Output

When compared to the two other scenarios analyzed, this one presents a much better match between the RE configuration and the number of installed ETS units. Indeed, there is just enough excess RE to charge the ETS heater at its rated power for most of the year and. Also, since the RE configuration has more WTs and fever PV than the other scenarios considered earlier, less excess RE will be wasted, mainly during the summer. Therefore, this allows the ETS unit to output a lot of heat during the colder months of the year which leads to substantial fuel savings.

Next, let us focus on combined results to compare different configurations. Figure 45 presents the heating oil savings obtained for all considered configurations. From down to top, each curve represents scenarios with 1 – 5 WTs. The left y-axis shows the total fuel savings obtained and the right on displays the percentage of fuel savings obtained for each home where Steffes 2103 is installed. As expected, the fuel savings increase when adding more and more RE, because it provides more available power for the ETS heaters to be charged. The first curve (red), from down to top, represents RE configurations with 1 WT while the last one (green) is for RE mixes with 5 WTs. The y-axis on the left of the figure represents the total fuel savings obtained by the ETS units while the one on the right of the figure refers to the percentage of fuel savings per home, where an ETS unit is installed.

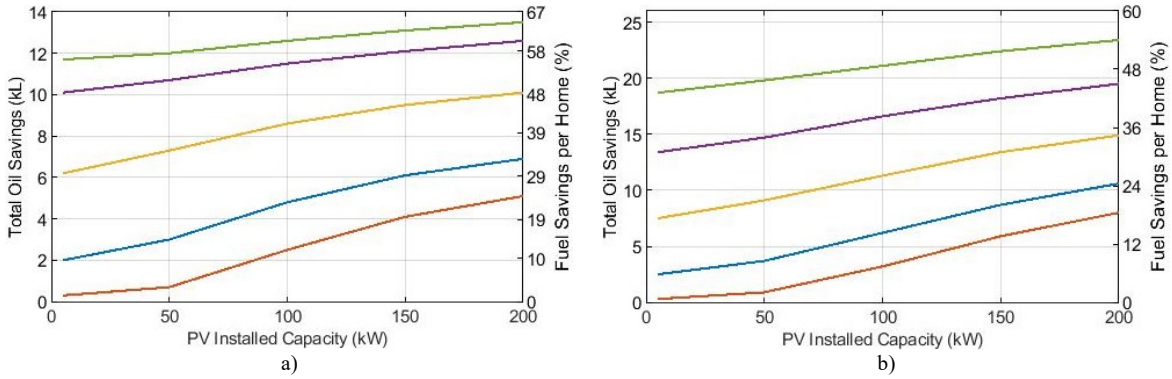

a) b)

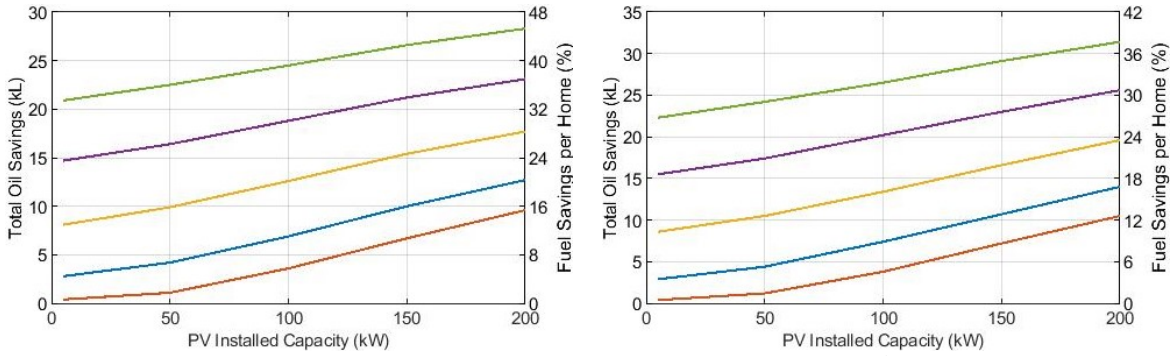

Figure 45 – Residential ETS Oil Savings: a) 10 ETS, b) 20 ETS, c) 30 ETS, d) 40 ETS.

One interesting result is that, for cases with ten ETS systems, the heating oil savings gain are much higher when going from two to three WTs than they are when adding a second, fourth or fifth WT. This observation will be further analyzed later in this section. On the other hand, when considering more ETS units, the gains obtained with a fourth or fifth WT are higher. Logically, RE configurations with more WTs and PV panels will provide more excess RE and are a better fit with configurations where a lot of ETS systems are installed. Also, with the current mix of RE considered, the potential heating oil consumption reduction for each home can reach 65% when 10 ETS units are installed and drops down to 38% for 40 ETS systems.

Then, Figure 46 shows the percentage of excess RE production recycled through space heating for all the RE configurations and for 10 to 40 installed ETS heaters.

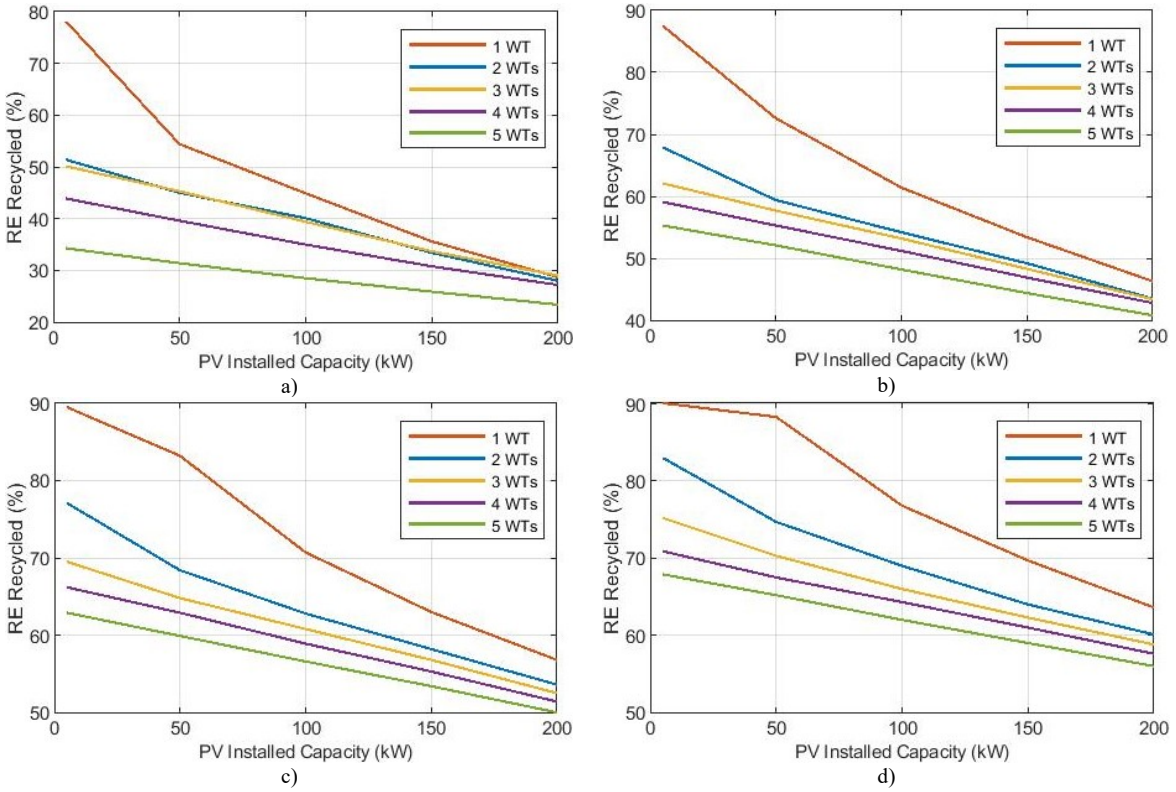

Figure 46 – Excess RE Recycled (%) by Residential ETS Units: a) 10 ETS, b) 20 ETS, c) 30 ETS, d) 40 ETS

As expected, the percentage of RE recycled is higher for configurations with less RE and when more ETS systems are considered. Another interesting observation is that increasing the number of installed PV reduces the percentage of excess RE recycled much more than when considering more WTs. For example, when observing Figure 46-b), one can notice that the excess RE recycled ranges from 40 to 50% for all scenarios with 200 kW of PV while the excess RE production of all configurations with only 5 kW of PV and up to 5 WTs is at least 55% and up to 88% recycled. More specifically, a configuration with 20 ETS units and 5 WTs + 5 kW of PV will recycle 55% of the excess RE generation vs. only 46% for a configuration with 1 WT + 200 kW PV even though the first one produces 80% more excess RE (337 MWh vs. 187 MWh). These results tend to support that wind energy is a better fit for space heating and follow the observations made in section 4.4.

To conclude, ETS systems supplied by excess RE can lead to important heating oil savings. However, to maximize their effectiveness, choosing the proper RE configuration and number of ETS units is key. First, in Arctic conditions, ETS units are better paired with WTs than they are with PV because the latter's production is concentrated during the warmer months and coincides with lower heating demand. RE configurations for which most of the energy is produced by PV panels will not produce a lot of excess RE during the colder months of the year when the heating demand is at its highest. Then, to ensure that ETS units operate at their full potential, it is important to allow each of the devices to charge at their maximum rating so they can maintain their SoC higher and output more heat. For example, if a certain RE configuration were to provide 55 kW or more of excess generation for most of the year, installing more than 10 Steffes 2103 units, with a total rated charging input of 54 kW, would not be recommended.

4.6. PV, Wind and ETS Combination Analysis

In this section, the results from sections 3.5 and 4.5 are combined and analyzed to assess the added effect of adding ETS units to the hybrid microgrid. Since scenarios with a fourth or fifth WT were introduced in section 4.5, Table 25 presents the initial low penetration simulation results for all the RE configurations considered for the ETS study. The results only include the initial curtailment and diesel savings before the addition of the ETS units. Also, Figure 47 displays the fuel savings obtained from those different RE mixes.

Table 25 – Diesel-PV-Wind Hybrid Microgrid Simulation Results

# WTs	Installed PV (kW)	RE Curtailed (%)	Diesel Savings (kL)	Diesel Savings (%)
1	5	4	29.3	16
	50	10	40.6	22
	100	24	46.3	25
	150	37	48.9	27
	200	46	50.5	27
2	5	18	46.4	25
	50	24	54.3	30
	100	33	58.1	32
	150	42	59.9	33

	200	49	61.0	33
3	5	35	53.7	29
	50	39	59.8	33
	100	45	62.9	34
	150	50	64.4	35
	200	55	65.4	36
4	5	48	57.0	31
	50	50	62.3	34
	100	54	65.2	35
	150	58	66.5	36
	200	61	67.4	37
5	5	57	58.9	32
	50	58	63.9	35
	100	60	66.5	36
	150	63	67.8	37
	200	66	68.6	37

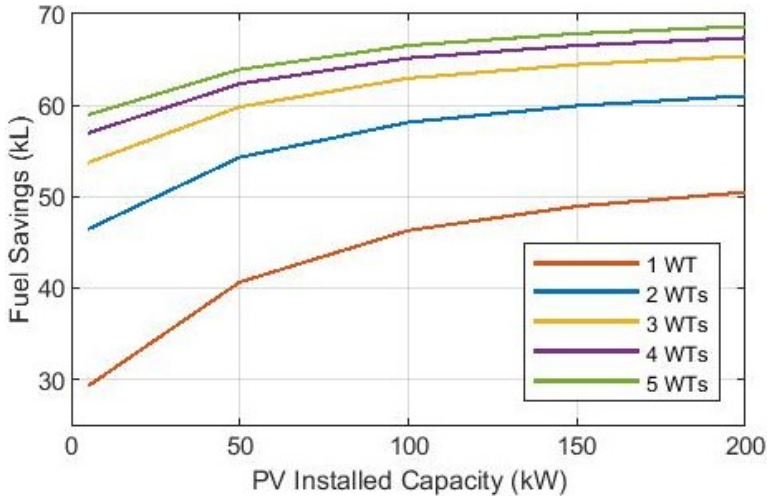

Figure 47 – Fuel Savings Simulation Results for Initial RE Study.

As mentioned in section 3.5, due to the increase in curtailment, the diesel fuel savings gains get notably smaller when adding more and more RE. It is especially notable that, when adding a third, fourth or fifth WT, the gains are much smaller than when adding a second one. Indeed, on average, adding a second WT will increase the fuel savings by 30%. That number goes down to 10%, 4% and 2% when adding a third, fourth or fifth WT.

Next, these results are combined with the ones from section 4.5. These combined results are all presented in Appendix I – Detailed RE and ETS Simulation Results. First, Figure 48 shows the effect of adding ETS units on the overall portion of RE that is curtailed, or in other words, wasted. Since ETS units are charged with excess RE generation, the net amount of energy curtailed can be represented by subtracting the amount of electrical energy supplied to the ETS units from the initial amount of energy that is curtailed. On each of the subplots, the hard lines represent the initial RE curtailment for all the configurations considered. The first curve (red), from down to top, represents RE configurations with 1 WT while the last one (green) is for RE mixes with 5 WTs. The dotted

lines represent the net RE curtailment for scenarios where ETS units are added alongside the RE mix.

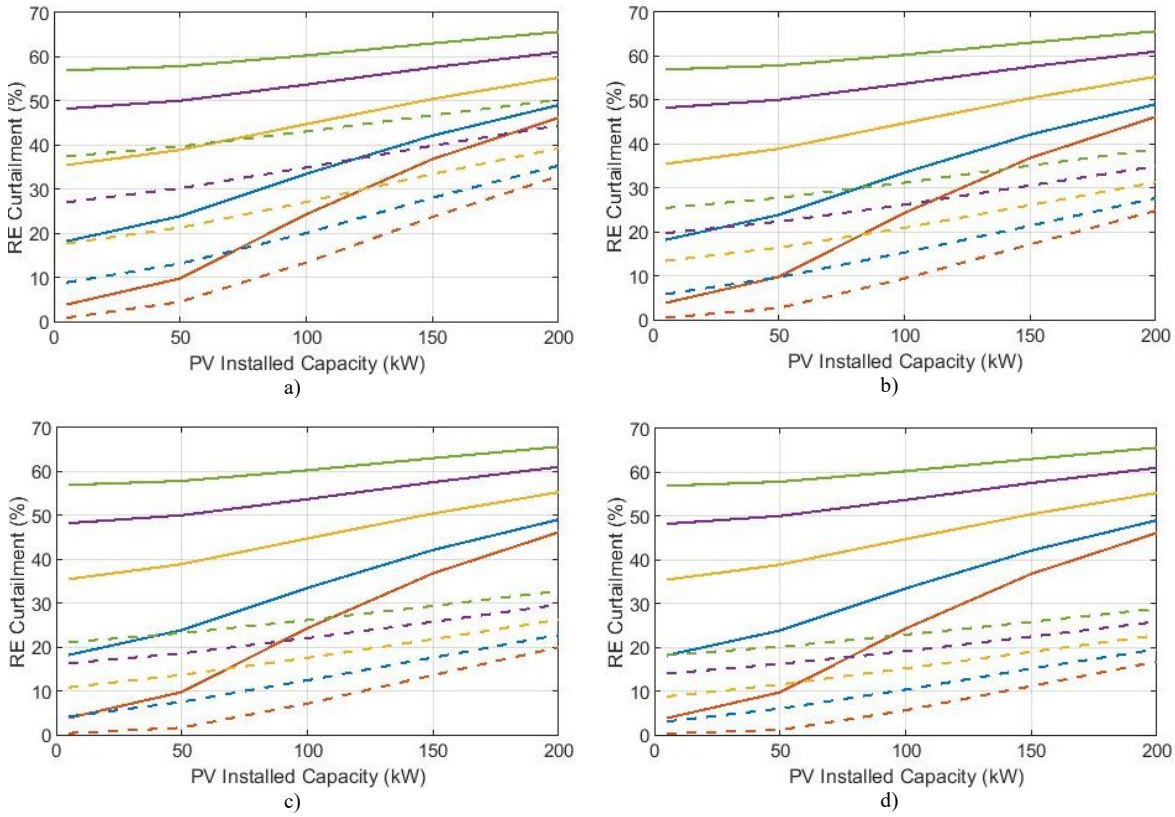

Figure 48 – Effect of ETS Units on RE Curtailment: a) 10 ETS, b) 20 ETS, c) 30 ETS, d) 40 ETS

From those results, one can note that adding ETS units has a substantial effect on reducing the curtailed RE generation. Even when adding ETS units, the curtailment remains substantial for some RE configurations, mainly when there is a lot of installed PV, since this excess generation is generally paired with periods of lower heating requirements. Next, Table 26 lists the average and maximum curtailment reduction when adding different numbers of installed ETS units. The maximum reduction in curtailment occurs for the RE configuration of 1 WT and 5 kW of PV.

Table 26 – Curtailment Reduction Statistics When Adding ETS Units

Number of ETS units	Average Reduction in Curtailment (%)	Maximum Reduction in Curtailment (%)
10	38	78
20	54	88
30	63	90
40	68	90

These results show that the efficiency of the RE systems will be increased because their curtailment or wasted energy is much lower. This will lead to much more energy supplied by RE and will also have a direct impact on the fossil fuel savings. Indeed, Figure 49 shows the effect of adding ETS units on the total fuel savings (diesel and heating oil) to the RE configurations. The diesel consumption from the gensets and the heating oil consumed by the ETS heaters are summed as total fuel consumed since they emit the same amount of GHG per litre [64], [65]. As for Figure 48,

the full lines represent the initial scenario with only RE while the dotted lines show the total fuel savings when adding ETS heaters.

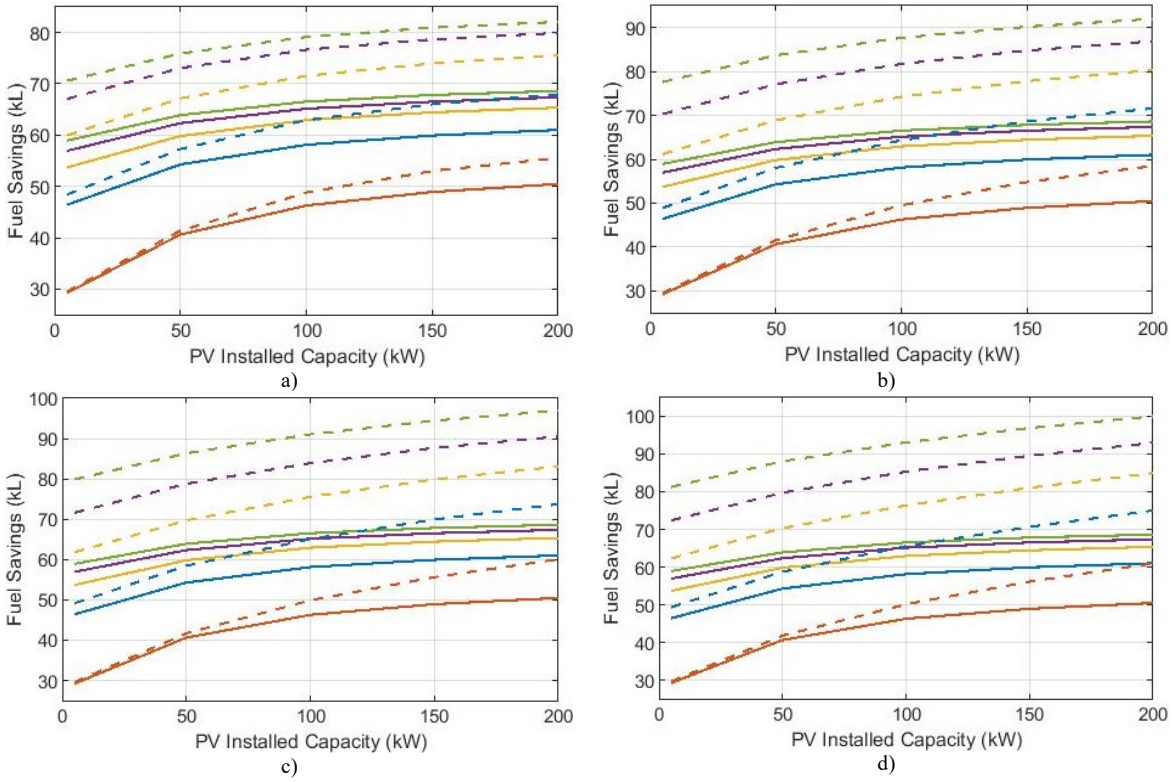

Figure 49 – RE and ETS Combined Fuel Savings: a) 10 ETS, b) 20 ETS, c) 30 ETS, d) 40 ETS

Then, Table 27 shows detailed fuel savings statistics for the configurations with ETS units. The maximum increase in fuel savings occurs for the RE configuration of 5 WTs + 200 kW PV for which the available excess RE to charge the ETS units is the highest.

Table 27 – Fuel Savings Increase Statistics When Adding ETS Units

Number of ETS units	Average Increase in Fuel Savings (%)	Maximum Increase in Fuel Savings (%)
10	13	20
20	19	34
30	22	41
40	24	46

These results show that the addition of ETS units has a clear effect on the total fuel savings of the community when compared to the ones obtained for RE supplying electrical loads only. First, if the objective were simply to maximize the total fuel savings, combining 5 WTs and 200 kW of PV with 40 ETS units would lead to total savings of 100.0 kL, which is 31.4 kL (46%) more than with PV and WTs only.

Then, the addition of ETS units leads to a much better increase in fuel savings when adding a third WT than it was the case in the original study. For example, the average gain in total fuels savings when adding a third WT ranges from 15%, with 10 ETS units, to 17% with 40 ETS heaters. With high numbers of ETS units installed, the fuel savings gain of adding a fourth or fifth WT becomes

more substantial. For example, with 40 ETS heaters, adding a fourth WT will lead to average gains of 12% while adding a fifth one will increase the savings by 9%.

Another interesting element to point out is that, when adding ETS units, the average slope of the fuel savings curves is much higher than it was in the original scenario. This suggests that the ETS units increase the yield of the PV system, by reusing its power generation, which was mostly curtailed and wasted in the first study. Indeed, with the added storage component, the PV generation can be converted to heat and stored during the day, when the outdoor temperature is higher, and then circulated in the houses at night, when the temperature drops, and the heating requirements increase. Therefore, the addition of storage could be beneficial for RE configurations with a lot of PV. For example, in the original study, when 3 WTs are installed with 200 kW of PV instead of 5 kW, it leads to an increase in diesel fuel savings of 11.7 kL. However, when combined with ETS units, going from a configuration of 3 WTs and 5 kW of PV to 3 WTs and 200 kW of PV leads to higher gains of total fuel savings, when combining both diesel and heating oil consumption. Indeed, it leads to additional savings of 15.5, 19.1, 21.3 and 22.6 kL when paired with 10,20,30 and 40 ETS units respectively.

Lastly, for all RE configurations equipped with 3 WTs and paired with 10 or more ETS units, the total fuel savings are higher than for any RE configurations, up to 5 WTs and 200 kW of PV, without any ETS heaters. Also, with 20 or more ETS units, it is possible to get more fuel savings than in with any configuration of the original study with only 2 WTs and 150 kW of PV (Figure 49-b),c),d) and further detailed in Appendix I – Detailed RE and ETS Simulation Results).

Next, Table 28 presents different RE configurations, with and without ETS units, which allow to obtain specific amounts of total fuel savings similarly to what was done in Table 19 in the first study.

Table 28 – Comparison of Total Fuel Savings Obtained for RE Configurations with and without ETS Units

Number of WTs	Installed PV (kW)	Number of ETS	Total Fuel Savings (kL)	RE Curtailment (%)
1	200	-	**50**	46
1	100	20		9
3	200	-	**65**	55
2	100	30		12
5	200	-	**69**	66
2	150	20		21
2	200	40	**75**	20
3	150	30	**80**	22
3	200	40	**85**	23
4	200	40	**93**	26
5	200	40	**100**	29

As seen in the first six rows of the table, adding ETS units to the microgrid allows to decrease the installed RE to obtain similar fuel savings with reduced RE capacity due to the substantial decrease in RE curtailment. Also, with the addition of ETS units, the potential for fuel savings is increased. As mentioned earlier, the addition of an ETS unit in each of the houses of the community (40) could lead to total fuel savings up to 46% higher than with RE only. The results of this study clearly show the potential and added value of ETS units for space heating electrification in remote Arctic

microgrids. Indeed, ETS heaters increase RE penetration and fuel savings while reducing RE curtailment. With the addition of ETS units to the microgrid, the potential for RE integration is higher. Indeed, it can supply both the initial electrical loads as well as the heating requirements, which represent a larger portion of the energy consumed and the GHG emissions of the community. These results therefore suggest that the electrification of heating should be a priority when trying to decarbonize remote Arctic communities.

When designing a hybrid microgrid in a real-life scenario to reduce the fuel consumption by a specific amount, it would most likely make more financial sense to include ETS units and limit the number of WTs installed. First, the capital cost of ten Steffes 2103 units represents just under 15% of the cost of a single Eocycle EOX S-16 WT [66], [67]. Next, shipping a WT is much more expensive than it is for ETS units. Shipping equipment to the Arctic is generally extremely expensive and depends on the size and on weight of the equipment. The WT considered in the study is generally shipped in a 40-foot container, which could fit around 100 Steffes 2103 without stacking them. In terms of weight, one EOX S-16 is equivalent to roughly 65 Steffes 2103, without considering the container. Then, installing, and operating WTs is more complex and expensive than it would be for heating systems. ETS units don't require specific maintenance while WT maintenance will be more expensive due to the cold climate. Further, the installation of WTs might require heavy machinery, such as a crane, which would also affect the shipping costs. Obviously, a more thorough assessment of the capital and O&M costs as well as the savings obtained from the fuel consumption reduction would be required to identify the optimal configuration of PV, WTs and ETS units for a remote Arctic microgrid. Also, since the heating demand is modelled in this study, having access to measured space heating data would be relevant. If a similar configuration were considered in a real-life scenario, measuring the oil consumption of several buildings with, for example, an hourly sampling rate, would be useful during the design process and would increase the accuracy of the potential fuel savings obtained when adding ETS units.

Chapter 5 - Conclusions

5.1. Summary

With the objective of increasing the RE penetration and reducing diesel fuel consumption in a small Canadian Arctic PV-Diesel hybrid microgrid, this work investigated the addition of wind energy to the microgrid, the combination of PV and wind in the microgrid and the implementation of methods which aimed to reduce PV curtailment. Before adding RE technologies, the remote microgrid considered in this study was powered solely by diesel gensets, which leads to a yearly consumption of 183.9 kL of fuel. With 2.5 kW - 200 kW of south-facing PV panels at an optimal tilt, yields a yearly PV penetration of 0.6 - 21.8% and fuel consumption of 183.0 - 151.3 kL. When considering the microgrid with WTs as its only source of RE, the penetration and the fuel consumption are 17.6% and 156.2 kL, 30.1% and 138.7 kL and 35.6% and 131.1 kL for one, two and three WTs, respectively. When combining the PV with up to three wind turbines, the RE penetration and the fuel consumption range from 18.1 - 44.3% and 155.4 - 118.5 kL, respectively. However, the increases in RE penetration without energy storage are associated with increases in curtailment, which is much more notable for PV than it is for wind. This is due to the fact that the load demand of the community is at its lowest when the PV produces most of its energy and vice versa.

New PV configurations, considering different panel tilts and orientations, with the objective of reducing PV curtailment and diesel fuel consumption, showed slight improvements in fuel consumption although the curtailment remained high. An East-West PV configuration was also considered and showed potential. However, it was set aside since a thorough techno financial analysis would be required to compare it to the other PV scenarios.

Considering the obtained results, one can conclude that the previous scenarios do not seem to be reasonable for medium or high RE penetration because of the high RE curtailment which makes the systems less effective (Table 19). Thus, the first part of the study shows the limit of the low penetration regime of RE in a remote Arctic microgrid.

Next, the second part of the study considers a new technology, alongside WTs and PV panels, to obtain a medium RE penetration configuration. The technology considered is electric thermal storage (ETS), which allows to recycle excess RE production to charge ETS units that store heat in high density bricks. The addition of those devices allows to reduce RE curtailment and oil heating consumption in buildings, which increases the efficiency of the installed WTs and PV panels. Also, the addition of a storage element allows to mitigate the issues related to the variability of the RE production as well as its mismatch, or delay, with the demand of the community. In this portion of the study, since the excess RE production can be recycled and the literature stated that WTs are a good fit for space heating requirements, the maximum number of WTs considered in the scenarios is increased from 3 to 5. The addition of ETS units to the PV-WT-Diesel hybrid microgrid results in substantial reductions in curtailment and overall fuel consumption. When

paring 10, 20, 30 or 40 ETS units, with 5 to 200 kW and 1 to 5 WTs, the RE curtailment is reduced on average by 38, 54, 63 and 68% (Table 26). These numbers of ETS units also increase the overall fuel savings on average by 13, 19, 22 and 24% (Table 27). For the configuration with the most RE installed considered in the study (5 WTs + 200 kW PV), the addition of 40 ETS units can provide an increase of fuel savings of 46% (Table 32). Also, when adding 40 ETS units to 1 WT + 5 kW PV, a reduction of 90% in RE curtailment is obtained (Table 26), which is the highest out of all the configurations considered. Lastly, pairing ETS units with the RE configurations considered can lead to residential oil heating savings of 65% for 10 houses (Figure 45-a)). If 40 houses are considered, the savings can reach 38% (Figure 45-e)).

Optimization is out of the scope of this study. However, it would be required to identify the optimal configuration of PV, WTs and ETS units for this specific setting. Some of the parameters that should be considered are: 1) the capital costs of the RE and ETS systems, including installation and shipping, 2) the O&M costs of the power plant, 3) the cost of diesel and 4) the GHG emissions.

Established approaches to optimize the sizing of PV and WTs already exist. A common method is the creation of a parametric objective function based on parameters similar to the ones aforementioned and the use of an optimization method to identify the best scenario [49], [50], [51]. These objectives functions generally aim to reduce the levelized cost of energy (LCOE), the sum of all the costs of an energy system over its lifetime divided by how much energy it produced, measured in $/kWh. Also, the reduction of GHG emissions is considered in those objective functions.

5.2. Future Work

First, since PV and WTs are intermittent sources of energy, it would be relevant to repeat the current study with solar and wind datasets from different Arctic communities to confirm whether these findings can be generalized.

Next, a similar study with a larger community size could be interesting because having a bigger load could give more flexibility for the sizing of RE systems. Indeed, it would be interesting to consider other types of WTs, for example in the 100 kW – 1 MW range to see their impact on a remote microgrid and assess which specific devices would be a better fit for specific wind profiles. Similarly, having access to more ETS experimental data would allow to compare the potential of different ETS units and assess how heaters with different input power ratings, storage capacity and number of charging elements could affect the fuel savings and net RE curtailment.

Also, since the method developed to generate the space heating profile of the community also allows to generate the water heating requirements, the electrification of that load could be an interesting next step.

Lastly, load-side management could also be considered to increase the match between RE production and loads such as heating requirements. For example, demand response control strategies could be developed to preheat buildings or water heaters when excess RE is available

and the ETS heaters can no longer be charged. However, this type of study would require further modelling to represent the thermal behaviour of buildings and water heaters.

Appendix I – Detailed RE and ETS Simulation Results

Table 29 – Detailed Combined Simulation Results – 10 ETS

# WTs	Installed PV (kW)	RE Diesel Savings (kL)	Initial RE Curtailed (%)	ETS Oil Savings (kL)	ETS Oil Savings (%)	Net RE Curtailed (%)	Total Fuel Savings (kL)	Total Fuel Savings Increase (%)
1	5	29.3	4	0.3	1	1	29.5	1
	50	40.6	10	0.7	4	4	41.4	2
	100	46.3	24	2.5	12	13	48.8	5
	150	48.9	37	4.1	20	24	53.0	8
	200	50.5	46	5.1	24	33	55.6	10
2	5	46.4	18	2.0	10	9	48.4	4
	50	54.3	24	3.0	14	13	57.3	6
	100	58.1	33	4.8	23	20	62.9	8
	150	59.9	42	6.1	29	28	66.0	10
	200	61.0	49	6.9	33	35	68.0	11
3	5	53.7	35	6.2	30	18	60.0	12
	50	59.8	39	7.3	35	21	67.2	12
	100	62.9	45	8.6	41	27	71.6	14
	150	64.4	50	9.5	46	33	74.0	15
	200	65.4	55	10.1	49	39	75.5	16
4	5	57.0	48	10.1	49	27	67.1	18
	50	62.3	50	10.7	52	30	73.1	17
	100	65.2	54	11.5	55	35	76.6	18
	150	66.5	58	12.1	58	40	78.7	18
	200	67.4	61	12.6	60	44	79.9	19
5	5	58.9	57	11.7	56	37	70.6	20
	50	63.9	58	12.0	58	40	75.9	19
	100	66.5	60	12.6	61	43	79.1	19
	150	67.8	63	13.1	63	47	80.9	19
	200	68.6	66	13.5	65	50	82.1	20

Table 30 – Detailed Combined Simulation Results – 20 ETS

# WTs	Installed PV (kW)	RE Diesel Savings (kL)	Initial RE Curtailed (%)	ETS Oil Savings (kL)	ETS Oil Savings (%)	Net RE Curtailed (%)	Total Fuel Savings (kL)	Total Fuel Savings Increase (%)
1	5	29.3	4	0.3	1	0	29.6	1
	50	40.6	10	0.9	2	3	41.6	2
	100	46.3	24	3.2	8	9	49.5	7
	150	48.9	37	5.9	14	17	54.8	12
	200	50.5	46	8.0	19	25	58.5	16
2	5	46.4	18	2.5	6	6	48.9	5
	50	54.3	24	3.7	9	10	58.0	7
	100	58.1	33	6.2	15	15	64.3	11
	150	59.9	42	8.7	21	21	68.6	15
	200	61.0	49	10.6	25	28	71.6	17
3	5	53.7	35	7.5	18	13	61.2	14
	50	59.8	39	9.1	22	16	68.9	15
	100	62.9	45	11.3	27	21	74.3	18
	150	64.4	50	13.4	32	26	77.8	21

	200	65.4	55	14.9	36	31	80.3	23
4	5	57.0	48	13.4	32	20	70.3	23
	50	62.3	50	14.7	35	22	77.1	24
	100	65.2	54	16.6	40	26	81.7	25
	150	66.5	58	18.2	44	31	84.8	27
	200	67.4	61	19.5	47	35	86.9	29
5	5	58.9	57	18.7	45	25	77.6	32
	50	63.9	58	19.8	48	28	83.7	31
	100	66.5	60	21.1	51	31	87.7	32
	150	67.8	63	22.4	54	35	90.2	33
	200	68.6	66	23.4	56	39	92.0	34

Table 31 – Detailed Combined Simulation Results – 30 ETS

# WTs	Installed PV (kW)	RE Diesel Savings (kL)	Initial RE Curtailed (%)	ETS Oil Savings (kL)	ETS Oil Savings (%)	Net RE Curtailed (%)	Total Fuel Savings (kL)	Total Fuel Savings Increase (%)
1	5	29.3	4	0.4	1	0	29.6	1
	50	40.6	10	1.1	2	2	41.7	3
	100	46.3	24	3.6	6	7	49.9	8
	150	48.9	37	6.7	11	14	55.6	14
	200	50.5	46	9.6	15	20	60.1	19
2	5	46.4	18	2.8	4	4	49.2	6
	50	54.3	24	4.2	7	8	58.4	8
	100	58.1	33	6.9	11	12	65.1	12
	150	59.9	42	10.0	16	18	69.9	17
	200	61.0	49	12.7	20	23	73.8	21
3	5	53.7	35	8.1	13	11	61.8	15
	50	59.8	39	9.9	16	14	69.7	17
	100	62.9	45	12.6	20	18	75.6	20
	150	64.4	50	15.4	25	22	79.9	24
	200	65.4	55	17.7	28	26	83.1	27
4	5	57.0	48	14.7	24	16	71.6	26
	50	62.3	50	16.4	26	19	78.8	26
	100	65.2	54	18.8	30	22	83.9	29
	150	66.5	58	21.2	34	26	87.7	32
	200	67.4	61	23.1	37	30	90.5	34
5	5	58.9	57	20.9	34	21	79.9	36
	50	63.9	58	22.5	36	23	86.4	35
	100	66.5	60	24.5	39	26	91.0	37
	150	67.8	63	26.6	43	29	94.4	39
	200	68.6	66	28.3	45	33	96.9	41

Table 32 – Detailed Combined Simulation Results – 40 ETS

# WTs	Installed PV (kW)	RE Diesel Savings (kL)	Initial RE Curtailed (%)	ETS Oil Savings (kL)	ETS Oil Savings (%)	Net RE Curtailed (%)	Total Fuel Savings (kL)	Total Fuel Savings Increase (%)
1	5	29.3	4	0.4	0	0	29.7	1
	50	40.6	10	1.2	1	1	41.8	3
	100	46.3	24	3.8	5	6	50.1	8
	150	48.9	37	7.2	9	11	56.1	15

	200	50.5	46	10.5	13	17	61.0	21
2	5	46.4	18	2.9	4	3	49.4	6
	50	54.3	24	4.4	5	6	58.7	8
	100	58.1	33	7.4	9	10	65.5	13
	150	59.9	42	10.7	13	15	70.7	18
	200	61.0	49	14.0	17	20	75.0	23
3	5	53.7	35	8.6	10	9	62.3	16
	50	59.8	39	10.5	13	12	70.3	18
	100	62.9	45	13.4	16	15	76.4	21
	150	64.4	50	16.6	20	19	81.0	26
	200	65.4	55	19.6	24	23	84.9	30
4	5	57.0	48	15.5	19	14	72.4	27
	50	62.3	50	17.4	21	16	79.7	28
	100	65.2	54	20.2	24	19	85.3	31
	150	66.5	58	23.0	28	22	89.5	35
	200	67.4	61	25.6	31	26	93.0	38
5	5	58.9	57	22.3	27	18	81.3	38
	50	63.9	58	24.2	29	20	88.1	38
	100	66.5	60	26.5	32	23	93.1	40
	150	67.8	63	29.1	35	26	96.9	43
	200	68.6	66	31.4	38	29	100.0	46

References

[1] Natural Resources Canada, “Clean Energy for Rural and Remote Communities Program.” [Online]. Available: https://natural-resources.canada.ca/reducingdiesel

[2] N. Ninad, D. Turcotte, and Y. Poissant, “Analysis of PV-Diesel Hybrid Microgrids for Small Canadian Arctic Communities,” *Canadian Journal of Electrical and Computer Engineering*, vol. 43, no. 4, pp. 315–325, 2020, doi: 10.1109/CJECE.2020.2995750.

[3] S. Srikumar, N. Ninad, and D. Turcotte, “PV Integration Study in a Canadian Northern Remote Community,” in *2020 47th IEEE Photovoltaic Specialists Conference (PVSC)*, Jun. 2020, pp. 1589–1596. doi: 10.1109/PVSC45281.2020.9300491.

[4] N. Ninad and D. Turcotte, “PV Utilization Analysis for a Canadian Small Arctic PV-Diesel Hybrid Microgrid,” in *2020 IEEE PESGM*, Montreal, QC, Canada, 2020.

[5] M. Brown, “Simulation and Optimization of High-Penetration Wind and Solar Energy for the Canadian High Arctic Research Station,” Master of Applied Science, Carleton University, Ottawa, Ontario, 2018. [Online]. Available: https://curve.carleton.ca/b3cd9b65-1cc3-4afe-b32c-f2ea51ec6e2b

[6] K. Solbakken, B. Babar, and T. Boström, “Correlation of wind and solar power in high-latitude arctic areas in Northern Norway and Svalbard,” *Renew. Energy Environ. Sustain.*, vol. 1, p. 42, 2016.

[7] M. R. Quitoras, P. E. Campana, and C. Crawford, “Exploring electricity generation alternatives for Canadian Arctic communities using a multi-objective genetic algorithm approach,” *Energy Conversion and Management*, vol. 210, p. 112471, 2020.

[8] S. Pelland, D. Turcotte, G. Colgate, and A. Swingler, “Nemiah Valley Photovoltaic-Diesel Mini-Grid: System Performance and Fuel Saving Based on One Year of Monitored Data,” *EEE Transactions on Sustainable Energy, volume 3, number 1*, pp. 167–175, Jan. 2012.

[9] Arctic Energy Alliance, “2018 ENERGY PROFILE.” 2020. [Online]. Available: https://aea.nt.ca/document/4246/?tmstv=1711483349

[10] F. Souba and P. B. Mendelson, “Chaninik Wind Group: Lessons learned beyond wind integration for remote Alaska,” *The Electricity Journal*, vol. 31, no. 6, pp. 40–47, Jul. 2018, doi: 10.1016/j.tej.2018.06.008.

[11] S. Wong and J.-P. Pinard, “Opportunities for Smart Electric Thermal Storage on Electric Grids With Renewable Energy,” *IEEE Transactions on Smart Grid*, vol. 8, no. 2, pp. 1014–1022, Mar. 2017, doi: 10.1109/TSG.2016.2526636.

[12] V. Chabot, “Faciliter la mise en oeuvre de l’accumulateur thermique électrique centralisé pour la gestion de la demande et la décarbonation du chauffage des bâtiments institutionnels,” ETS Montréal. [Online]. Available: https://espace.etsmtl.ca/id/eprint/3233/1/CHABOT_Vincent.pdf

[13] K. D’Avignon, “Stockage thermique et exemplarité de l’État,” ÉTS Montréal, V. 2022-03-15, 2022. [Online]. Available: https://transitionenergetique.gouv.qc.ca/fileadmin/medias/pdf/publications/ETS-Stockage-thermique-exemplarite-Etat.pdf

[14] P. S. Sauter, B. V. Solanki, C. A. Cañizares, K. Bhattacharya, and S. Hohmann, “Electric Thermal Storage System Impact on Northern Communities’ Microgrids,” *IEEE Transactions on Smart Grid*, vol. 10, no. 1, pp. 852–863, Jan. 2019, doi: 10.1109/TSG.2017.2754239.

[15] M. A. Moffet, F. Sirois, G. Joós, and A. Moreau, “Central electric thermal storage (ETS) heating systems: Impact on customer and distribution system,” in *PES T&D 2012*, May 2012, pp. 1–7. doi: 10.1109/TDC.2012.6281536.
[16] Steffes, “Electric Thermal Storage,” Steffes. Accessed: Oct. 12, 2023. [Online]. Available: https://steffes.com/ets/
[17] Hydro-Québec, “Les accumulateurs thermiques locaux en remplacement des plinthes électriques dans les bâtiments commerciaux.” 2020.
[18] J. Date, J. A. Candanedo, A. K. Athienitis, and K. Lavigne, “Development of reduced order thermal dynamic models for building load flexibility of an electrically-heated high temperature thermal storage device,” *Science and Technology for the Built Environment*, vol. 26, no. 7, pp. 956–974, Aug. 2020, doi: 10.1080/23744731.2020.1735260.
[19] Centre de recherche d’Hydro-Québec (CRHQ) - Laboratoire des technologies de l’énergie (LTE), “Intégration du stockage thermique dans les réseaux autonomes: simulation d’un appareil de chauffage local avec accumulation thermique,” 2017.
[20] Canadian Association of Petroleum Producers, “Petroleum in Real Life: Home heating - Context Magazine by CAPP,” https://context.capp.ca/. Accessed: Sep. 25, 2023. [Online]. Available: https://context.capp.ca/articles/2021/petroleum-in-real-life-home-heating/
[21] Environment and Climate Change Canada, “Engineering Climate Datasets.” [Online]. Available: https://climate.weather.gc.ca/prods_servs/engineering_e.html
[22] A. U. Obiwulu, N. Erusiafe, M. A. Olopade, and S. C. Nwokolo, “Modelling and estimation of the optimal tilt angle, maximum incident solar radiation, and global radiation index of the photovoltaic system,” *Heliyon*, vol. 8, no. 6, p. e09598, 2022.
[23] S. Canada, “Weather, climate and hazards.” [Online]. Available: https://www.canada.ca/en/services/environment/weather.html
[24] F. Sheriff, D. Turcotte, and M. Ross, “PVToolbox v.1a - Programmer’s Notes,” in *Report # 2003-096 (TR), CanmetENERGY*, Natural Resources Canada, 2003.
[25] N. Ninad, D. Turcotte, and Y. Poissant, *Energy Benchmark Study for Northern Remote Microgrids*. 2016.
[26] California Energy Commission, “Utility Interactive Inverter List (Full Data).” 2020. [Online]. Available: https://www.energy.ca.gov/sites/default/files/2020-06/Utility_Interactive_Inverter_List_Full_Data.xlsm.
[27] Enphase Energy, “M250-60-2LL-S22.” [Online]. Available: https://www.renvu.com/ENPHASE-ENERGY-M250-60-2LL-S22-60-Cell-250W-240-208-VAC-MC4#:~:text=The%20M250%20is%20rated%20at,in%20the%20industry%20for%20microinverters.
[28] Eclipsall Energy Corp., “NRG 60M 250W - 275W Datasheet.” [Online]. Available: https://www.enfsolar.com/Product/pdf/Crystalline/51f88a6fbd872.pdf
[29] Eocycle, “EOX S-16 Datasheet.” 2023. [Online]. Available: https://eocycle.com/wp-content/uploads/2021/05/15064-EocycleMerger-SpecSheet-S16-R5.pdf.
[30] O. Ulleberg, “Stand-alone power systems for the future: Optimal design, operation and control of solar-hydrogen energy systems.” 1998. [Online]. Available: https://www.osti.gov/etdeweb/biblio/353163.
[31] R. Pena, R. Cardenas, J. Proboste, J. Clare, and G. Asher, “Wind–Diesel Generation Using Doubly Fed Induction Machines,” *Energy Conversion, IEEE Transactions on*, vol. 23, pp. 202–214, 2008.

[32] UPS Systems, “Can you low load a diesel generator?” [Online]. Available: https://www.upssystems.co.uk/blog/post/low-load-diesel-generator
[33] Kohler - SDMO Controls, “APM403 COMMAND/CONTROL Datasheet.” [Online]. Available: http://www.genpowerusa.com/content/files/DATASHEET-SDMO-CONTROL-APM403.pdf
[34] Schneider Electric, “Excess photovoltaic production - how to manage.” [Online]. Available: https://www.electrical-installation.org/enwiki/Excess_photovoltaic_production_-_how_to_manage
[35] Schneider Electric, “CL Series Inverter: Application Note on Export Limiting.” 2021. [Online]. Available: https://solar.se.com/eu/wp-content/uploads/sites/4/2021/11/CL-Export-Limiting-Application-Note_990-91524.pdf
[36] Leading Edge Turbines & Power Solutions, “How diversion charge controllers and dump loads work.” [Online]. Available: https://www.leadingedgepower.com/news/2013/how-diversion-charge-controllers-and-dump-loads-work.html
[37] Mita-Teknik, “WP4100 MK ll Controller.” [Online]. Available: https://www.mita-teknik.com/media/1144/wp4x00.pdf
[38] C. Stanciu and D. Stanciu, “Optimum tilt angle for flat plate collectors all over the World – A declination dependence formula and comparisons of three solar radiation models,” *Energy Conversion and Management*, vol. 81, pp. 133–143, 2014.
[39] RatedPower, “Simulating east-west configurations with pvDesign.” [Online]. Available: https://ratedpower.com/blog/east-west-solar-panels/
[40] *Old Crow Solar Project with ATCO*, (Mar. 20, 2023). Accessed: May 16, 2024. [Online Video]. Available: https://www.youtube.com/watch?v=EoSTk_njztQ
[41] Atco Electric, “OLD CROW SOLAR PROJECT.” Accessed: May 16, 2024. [Online]. Available: https://electric.atco.com/en-ca/community/projects/old-crow-solar-project.html
[42] ECGSOLAX, “The Advantages of Multiple MPPTs in Solar Inverters,” ECGSOLAX. Accessed: May 17, 2024. [Online]. Available: https://www.ecgsolax.com/blogs/for-beginners/the-advantages-of-multiple-mppts-in-solar-inverters
[43] SPW, “Dual MPPT Defined, Understanding Solar MPPT,” Solar Power World. Accessed: May 17, 2024. [Online]. Available: https://www.solarpowerworldonline.com/2014/02/dual-mppt-defined-understanding-mppt/
[44] Prairie Sun Solar, “Shop,” Prairie Sun Solar. Accessed: May 15, 2024. [Online]. Available: https://prairiesunsolar.com/shop/
[45] Solar Power Depot, “Shop | Solar Power Depot.” Accessed: May 15, 2024. [Online]. Available: https://solarpowerdepot.ca/shop/
[46] SMA America, “Sunny Boy 3.0-US - 7.7-US | SMA America.” Accessed: May 15, 2024. [Online]. Available: https://www.sma-america.com/products/solarinverters/sunny-boy-30-us-41-77-us-41
[47] “Fronius Primo 3.8-1 208-240.” Accessed: May 15, 2024. [Online]. Available: https://www.fronius.com/en-ca/canada/solar-energy/installers-partners/technical-data/all-products/inverters/fronius-primo/fronius-primo-3-8-1-208-240
[48] I. Das and C. Cañizares, “Renewable Energy Development in Canadian Arctic - Phase II: Feasability Studies Report on Selected Communities of Nunavut and Northwest Territories,” Waterloo Institute of Sustainable Energy (WISE), 2016. [Online]. Available: https://wwf.ca/wp-content/uploads/2020/03/Fuelling-change-in-the-arctic_2016.pdf
[49] M. Kalogera and P. Bauer, “Optimization of an off-grid hybrid system for supplying offshore platforms in arctic climates,” in *2014 International Power Electronics Conference*

(IPEC-Hiroshima 2014 - ECCE ASIA), May 2014, pp. 1193–1200. doi: 10.1109/IPEC.2014.6869738.
[50] T.-T. Nguyen and T. Boström, "Multiobjective Optimization of a Hybrid Wind/Solar Battery Energy System in the Arctic," *Journal of Renewable Energy*, vol. 2021, pp. 1–11, Apr. 2021, doi: 10.1155/2021/8829561.
[51] A. Lavrik, Y. Zhukovskiy, and A. Buldysko, "Features of the Optimal Composition Determination of Energy Sources During Multi-Criterial Search in the Russian Arctic Conditions," in *2020 International Youth Conference on Radio Electronics, Electrical and Power Engineering (REEPE)*, Mar. 2020, pp. 1–5. doi: 10.1109/REEPE49198.2020.9059215.
[52] Office of Energy Efficiency & Renewable Energy, "Prototype Building Models | Building Energy Codes Program." Accessed: Sep. 25, 2023. [Online]. Available: https://www.energycodes.gov/prototype-building-models
[53] I. Maynard and A. Abdulla, "Estimating thermal energy loads in remote and northern communities to facilitate a net-zero transition," *Environ. Res.: Infrastruct. Sustain.*, vol. 3, no. 1, p. 011001, Feb. 2023, doi: 10.1088/2634-4505/acb3f4.
[54] N. R. C. Government of Canada, "Residential Sector Territories1 Table 2: Secondary Energy Use and GHG Emissions by End-Use." Accessed: May 02, 2024. [Online]. Available: https://oee.nrcan.gc.ca/corporate/statistics/neud/dpa/showTable.cfm?type=CP&sector=res&juris=tr&year=2021&rn=2&page=0
[55] Natural Resources Canada, "Oil-fired water heaters - household." Accessed: Sep. 26, 2023. [Online]. Available: https://natural-resources.canada.ca/energy-efficiency/energy-efficiency-regulations/guide-canadas-energy-efficiency-regulations/oil-fired-water-heaters-household/6899
[56] Natural Resources Canada, "Heating With Oil," 2012. [Online]. Available: https://natural-resources.canada.ca/sites/nrcan/files/energy/pdf/energystar/Heating-with-Oil_EN.pdf
[57] Steffes, "Private Communication Regarding Steffes 2103 Specifications," 2023.
[58] Centre de recherche d'Hydro-Québec (CRHQ) - Laboratoire des technologies de l'énergie (LTE), "Utilisation des accumulateurs thermiques locaux (ATL) au LTE pour gérer la demande en puissance et offrir des services énergétiques au réseau: résultats de l'hiver 2019-2020," 2020.
[59] Steffes, "Owner's and Installer's Manual for Room Heating Units." [Online]. Available: https://www.google.com/url?sa=i&url=https%3A%2F%2Fwww.steffes.com%2Fwp-content%2Fuploads%2F2016%2F09%2FOwnersManual-1.pdf&psig=AOvVaw0OYh8h1EZarJXrtEVF6eVu&ust=1709316445208000&source=images&cd=vfe&opi=89978449&ved=0CAYQn5wMahcKEwjw5KOPktGEAxUAAAAAHQAAAAAQDA
[60] Steffes, "STEFFES MASTER SUPPLEMENTAL INSTALLER'S GUIDE FOR 2100, 3100, 4100 and 5100 SERIES."
[61] G. Bolt, M. Wilber, D. Huang, D. J. Sambor, S. Aggarwal, and E. Whitney, "Modelling and Evaluating Beneficial Matches between Excess Renewable Power Generation and Non-Electric Heat Loads in Remote Alaska Microgrids," *Sustainability*, vol. 14, no. 7, p. 3884, Mar. 2022, doi: 10.3390/su14073884.
[62] H. G. Beyer and B. A. Niclasen, "Assessment of the option 'wind power to heat for buildings' with respect to meteorological conditions," *Meteorologische Zeitschrift*, pp. 79–85, Mar. 2019, doi: 10.1127/metz/2019/0940.

[63] Y. Li, V. G. Agelidis, and Y. Shrivastava, “Wind-solar resource complementarity and its combined correlation with electricity load demand,” in *2009 4th IEEE Conference on Industrial Electronics and Applications*, May 2009, pp. 3623–3628. doi: 10.1109/ICIEA.2009.5138882.
[64] Natural Resources Canada, “Learn the facts: Emissions from your vehicle,” 2014. [Online]. Available: https://natural-resources.canada.ca/sites/www.nrcan.gc.ca/files/oee/pdf/transportation/fuel-efficient-technologies/autosmart_factsheet_9_e.pdf
[65] U.S. Energy Information Administration, “Carbon Dioxide Emissions Coefficients.” Accessed: Sep. 27, 2023. [Online]. Available: https://www.eia.gov/environment/emissions/co2_vol_mass.php
[66] Eocycle, “Private Communication Regarding the Specifications and Cost of the EOX S-16 Wind Turbine,” 2023.
[67] Le Groupe Master, “Private Communication Regarding the Cost of Steffes ETS Units,” 2024.